Supplementary Tables

Table S1. Quality metrics of RNA-seq libraries

Table S2. Normalized gene expression values of all detected genes in all samples used

Table S3. Differential gene expression between the quiescent and activated neural lineage populations

Table S4. Differential gene expression within and between individual quiescent and activated neural lineage populations

Table S5. Differentially expressed KEGG pathways between quiescent and activated neural lineage populations

Table S6. Differential expression of proteasome, lysosome, and protein chaperone genes between quiescent and activated neural lineage populations

Table S7. Differential gene expression with age in 5 cell types from the regenerative region of the brain: endothelial cells, astrocytes, quiescent neural stem cells, activated neural stem cells, and neural progenitor cells

Table S8. Differential KEGG pathway expression with age in 5 cell types from the regenerative region of the brain: endothelial cells, astrocytes, quiescent neural stem cells, activated neural stem cells and neural progenitor cells

Supplementary Figure Legends

Fig. S1. Validation of neural stem cell FACS-sorting protocol

A) FACS sorting scheme used to isolate cells from the SVZs of young and old GFAP-GFP mice. Negative controls for staining are indicated. Each negative control sample was stained with all antibodies other than the one(s) for which it was the negative control.

B) Reverse-transcription followed by quantitative PCR (RT-qPCR) validation of mRNA marker expression in the 4 neural lineage populations isolated from SVZs of young and old mice. C(t) values in linear scale are normalized to 18S rRNA and scaled to the range [0, 1].

C) Cell cycle distribution is as expected and unchanged with age in the endothelial and four neural lineage populations FACS-sorted from the SVZs of young or old mice. Cell cycle is measured by injecting mice with EdU, which is incorporated into DNA during S-phase, 2 hours before SVZ dissection and FACS. EdU levels were detected by fluorescent click-chemistry and DNA content was detected by propidium iodide (PI). Cell cycle distribution of each population with regard to EdU and PI was measured by flow cytometry. Cells in G0/G1 were defined as EdU^- and PI^{low} (1n DNA), cells in S-phase were defined as EdU^+PI^{mid}, and cells in G2/M were defined as PI^{high} (2n DNA).

Fig. S2. Quality analysis of the RNA-seq libraries

A) There is no observable batch effect by sequencing lane. Principal component analysis (PCA) of all 35 RNA-seq samples, based on VST-normalized read counts (variance stabilizing transformation, implemented in DESeq2) of all detected genes. The samples were sequenced on 10 sequencing lanes, which are represented by 10 different colors.

B) There is a subtle batch effect by FACS-sorting day, and this is accounted for in the statistical models used for further analysis. Principal component analysis (PCA) of all 35 RNA-seq samples, based on VST-normalized read counts of all detected genes. The samples were FACS-sorted on four different days, which are represented by 4 different colors.

C) Expression of markers for astrocytes and quiescence (top), proliferation and neurogenesis (middle), and endothelial and hematopoietic lineages (bottom). Shown are the VST-normalized read counts, accounting for the day of FACS and scaled to the range [0, 1]. The hematopoietic markers CD45 and PU.1 were not expressed, thus normalized expression values cannot be shown (these genes did not pass the gene-filtering step of minimum 2 samples with minimum 2 read counts per million mapped reads and were therefore excluded from the dataset before the data were normalized).

D) Unsupervised hierarchical clustering of all 35 RNA-seq samples. The hierarchical clustering (average linkage) was performed based on 1 - Spearman's rank correlation on VST-normalized read counts (variance stabilizing transformation, implemented in DESeq2) of all detected genes, accounting for the day of FACS.

Fig. S3. Quiescent and activated neural lineage populations of the SVZ exhibit differential homeostatic signatures

A) Transcriptional differences in homeostatic KEGG pathways between quiescent and activated neural stem cells in young adult mice. For a listing of all differentially expressed KEGG pathways, see Table S5. Differential expression of KEGG pathways was evaluated by calculating the arithmetic mean of gene-wise test statistics (Wald test

statistic from differential expression analysis using DESeq2) per pathway. p-values were obtained by bootstrap sampling and corrected for multiple hypothesis testing using the Benjamini-Hochberg algorithm. * FDR-adjusted $p \leq 0.05$, ** FDR-adjusted $p \leq 0.001$, *** FDR-adjusted $p \leq 0.0001$. X-axis shows the mean of log2 fold changes of activated vs. quiescent neural stem cells for all genes in this pathway.

B) Transcriptional differences in homeostatic KEGG pathways between quiescent neural lineage populations (astrocytes and qNSCs) and activated neural lineage populations (aNSCs and NPCs) in young mice. Shown are the differential expression results of the same KEGG pathways as in Fig. S3A, for the comparison of old quiescent and old activated neural lineage populations. Differential expression of KEGG pathways was evaluated by calculating the arithmetic mean of gene-wise test statistics (Wald test statistic from differential expression analysis using DESeq2) per pathway. p-values were obtained by bootstrap sampling and corrected for multiple hypothesis testing using the Benjamini-Hochberg algorithm. * FDR-adjusted $p \leq 0.05$, ** FDR-adjusted $p \leq 0.001$, *** FDR-adjusted $p \leq 0.0001$. X-axis shows the mean of log2 fold changes of activated vs. quiescent neural lineage populations for all genes in this pathway. For a listing of all differentially expressed KEGG pathways, see Table S5.

C) Transcriptional differences in homeostatic KEGG pathways between quiescent and activated neural stem cells in old mice. Shown are the differential expression results of the same KEGG pathways as in Fig. S3, A and B, for the comparison of old qNSCs and old aNSCs. Differential expression of KEGG pathways was evaluated by calculating the arithmetic mean of gene-wise test statistics (Wald test statistic from differential expression analysis using DESeq2) per pathway. p-values were obtained by bootstrap

sampling and corrected for multiple hypothesis testing using the Benjamini-Hochberg algorithm. * FDR-adjusted $p \leq 0.05$, ** FDR-adjusted $p \leq 0.001$, *** FDR-adjusted $p \leq 0.0001$. X-axis shows the mean of log2 fold changes of activated vs. quiescent neural stem cells for all genes in this pathway. For a listing of all differentially expressed KEGG pathways, see Table S5.

D) Transcriptional differences in homeostatic KEGG pathways between quiescent neural lineage populations (astrocytes and qNSCs) and activated neural lineage populations (aNSCs and NPCs) in old mice. Shown are the differential expression results of the same KEGG pathways as in Fig. S3, A to C, for the comparison of old quiescent and old activated neural lineage populations. Differential expression of KEGG pathways was evaluated by calculating the arithmetic mean of gene-wise test statistics (Wald test statistic from differential expression analysis using DESeq2) per pathway. p-values were obtained by bootstrap sampling and corrected for multiple hypothesis testing using the Benjamini-Hochberg algorithm. * FDR-adjusted $p \leq 0.05$, ** FDR-adjusted $p \leq 0.001$, *** FDR-adjusted $p \leq 0.0001$. X-axis shows the mean of log2 fold changes of activated vs. quiescent neural lineage populations for all genes in this pathway. For a listing of all differentially expressed KEGG pathways, see Table S5.

Fig. S4. Analysis of genes differentially regulated between quiescent and activated stem cells

A) Transcriptional differences in homeostatic KEGG pathways between quiescent and activated NSCs grown in culture (*in vitro;* data from Martynoga *et al.* 2013 (*18*)). Shown are the differential expression results of the same KEGG pathways as in Fig. S3, for the

comparison of qNSCs and aNSCs *in vitro*. Up- and down-regulation of KEGG pathways was evaluated by calculating the arithmetic mean of gene-wise test statistics (Wald test statistic from differential expression analysis using DESeq2) per pathway. p-values were obtained by bootstrap sampling and corrected for multiple hypothesis testing using the Benjamini-Hochberg algorithm. * FDR-adjusted $p \leq 0.05$, ** FDR-adjusted $p \leq 0.001$, *** FDR-adjusted $p \leq 0.0001$.

B) Transcriptional differences in proteostatic pathways between quiescent and activated neural lineage populations (data from Codega *et al.* 2014 (*7*)). Heatmap showing all genes in pathways relevant to the three main branches of proteostasis: lysosome (KEGG), proteasome (KEGG), and chaperone proteins (chaperone list compiled from Uniprot and Gene Ontology, see Materials and Methods for details). Expression is depicted as normalized microarray intensities, and scaled row-wise.

C) Top panel: An E-box/bHLH (TFEB) motif was identified as the only transcription factor motif significantly enriched in the promoter regions of qNSC lysosomal genes by the software HOMER, testing for enrichment of all known motifs (see Materials and Methods for details). Note that an E-box/bHLH motif could be recognized by other bHLH transcription factors. p-value was calculated in HOMER using a binomial statistical test. Bottom panel: Transcriptional differences in all TFEB target genes between quiescent and activated neural lineage populations. Heatmap showing expression of TFEB ChIP-seq target genes (*17*) in quiescent and activated neural lineage populations. Expression is depicted as VST-normalized read counts, taking into account the day of FACS, and scaled row-wise. Differential expression of TFEB ChIP-seq target genes between young adult quiescent and activated neural lineage populations was

evaluated by calculating the arithmetic mean of gene-wise test statistics (Wald test statistic from differential expression analysis using DESeq2) for this gene set. p-value was obtained by bootstrap sampling.

D) Ingenuity Pathways Analysis (IPA) of predicted upstream regulators of the transcriptome-wide differences between quiescent and activated NSCs *in vivo*. Plotted are the Z-scores of the top 5 most significant transcription factors predicted to drive the transcriptional signatures in qNSCs and aNSCs, filtered for transcription factors expressed in the dataset, with $p < 0.05$ and absolute Z-score > 2. Note that IPA does not correct p-values for multiple hypothesis testing.

E) Differences in expression of specific subsets of protein chaperones between quiescent and activated neural lineage populations. Heatmap showing all genes in the endoplasmic reticulum (ER) unfolded protein response pathway (Gene Ontology pathway GO0030968), and all subunits of the prefoldin and TCP-1 ring complex (TRiC) complexes. Expression is depicted as VST-normalized read counts, taking into account the day of FACS, and scaled row-wise. The list of genes in each of these pathways and their differential expression between quiescent and activated populations can be found in Table S6.

F) Transcriptional differences in proteostasis pathways between quiescent and activated stem cells from other adult tissues. Heatmaps showing all genes in the proteasome pathway (KEGG), lysosome pathway (KEGG), and chaperone protein pathway (chaperone list compiled from Uniprot and Gene Ontology, see Materials and Methods) for quiescent and activated muscle stem cells (qMuSC and aMuSC, respectively; left) and

hematopoietic stem cells (LT-HSC and ST-HSC, respectively; right). Expression is depicted as normalized microarray intensities and scaled row-wise.

Fig. S5. Lysosome and proteasome activity in quiescent and activated neural stem cells

A) Whole mount staining of a young adult (3-month-old) brain SVZ indicates more lysosomes in quiescent than activated NSCs. Left panel: Representative SVZ field of view. qNSCs/astrocytes are labeled by GFAP (red) and aNSC/NPC nuclei are labeled by Ki67 (green). Lysosomes are labeled by Lamp-1 (yellow), and nuclei are labeled with DAPI (blue). Arrows (white) point to an example of a qNSC/astrocyte (Q) and an example of an aNSC/NPC nucleus (A). Scale bar represents 5 μm. Right panel: Quantification of Lamp-1 antibody staining by cell type. Cells were unbiasedly selected based upon a DAPI nuclei stain beneath the ependymal cell layer, then binned into aNSC/NPCs or qNSCs/astrocytes using Ki67 and GFAP staining as markers, respectively. Lamp-1 staining intensity was then quantified for each individual cell (n = 100 over 3 animals), and normalized for cell size. p-value was calculated by the two-sided Wilcoxon rank-sum test. *$p \leq 0.05$.

B) Differences in Lamp-2^+ area quantified from images of 5 independent biological replicates indicate a statistically significant difference between primary cultures of qNSCs and aNSCs (right panel). Each point represents one independent primary culture derived from two 3-4-month-old mice analyzed on two different days. Note that the quiescent cell data are also part of Fig. S7B. Bars represent mean -/+ sem of values from

5 independent primary cultures. p-values were calculated using the one-sided Wilcoxon rank-sum test. * $p \leq 0.05$.

C) Relative autolysosome levels in primary cultures of mCherry-GFP-LC3$^+$ qNSCs and aNSCs, measured by flow cytometry (schematic in Fig. 1H). Y-axis represents the median of the ratios of mCherry to GFP fluorescence per cell in each biological replicate normalized to the median value on the day of measurement (to combine independent experiments). Bars represent mean -/+ sem of values from 6 independent biological replicates analyzed on 2 different days. p-value was calculated using the two-sided Wilcoxon rank-sum test. *** $p \leq 0.001$.

D) qNSCs exhibit slower autophagic flux than aNSCs freshly isolated from the adult brain. Top panel: Schematic illustration of experimental setup. Four cell types were FACS-sorted from the SVZ and incubated for 2 hours under basal conditions, or with one of two independent inhibitors of lysosomal acidification, Bafilomycin A (BafA) or Chloroquine. The increase in median LC3 levels in the drug-treated conditions compared to basal conditions for each cell type was calculated as a measure of the degree of autophagic flux over the 2 hours of treatment. Bottom panel: Y-axis represents the increase in median LC3 protein levels after 2 hours of treatment with 400 nM Bafilomycin A (BafA) or Chloroquine, measured by intracellular flow cytometry. Each point represents FACS-sorted cells from a single mouse. Mean -/+ sem of values from 3 different mice (3-4 months old) analyzed on the same day. p-values were calculated using the one-sided Wilcoxon rank-sum test. * $p \leq 0.05$.

E) Quiescent NSCs exhibit lower levels of conjugated ubiquitin than activated NSCs directly isolated from the SVZ. The Y-axis represents the median fluorescence per cell of

conjugated ubiquitin normalized to cell size (forward scatter) and normalized to the median conjugated ubiquitin fluorescence value for each mouse analyzed, to compare between mice. Each point represents FACS-sorted cells from a single mouse. Mean -/+ sem of values from 4 different mice (3-4 months old) analyzed on a single day. p-value was calculated using the two-sided Wilcoxon rank-sum test. * $p \leq 0.05$.

F) aNSCs exhibit more chymotrypsin-like proteasome activity than qNSCs in primary cultures. Chymotrypsin-like proteasome activity is measured by fluorescence of 7-Amino-4-methylcoumarin (AMC) generated from cleavage of AMC-conjugated proteasome substrate (Succ-LLVY-AMC) by lysates from qNSCs or aNSCs. Non-specific fluorescence, as determined by incubating each lysate with the proteasome-inhibitor MG132, is subtracted from the values. Values are normalized to the median fluorescence reading on the day of each assay. X-axis represents the time that lysates were incubated with substrate. Points represent mean and bars represent -/+ standard error of the mean (sem) of 5 independent NSC cultures from two different experiment days. p-value was calculated using the one-sided Wilcoxon rank-sum test comparing the areas under the curves for all replicates. ** $p \leq 0.01$.

Fig. S6. Protein aggregates in qNSCs and aNSCs

A) Quiescent and activated neural stem cells use different branches of the proteostasis network, raising the question of how these cells differ in their proteome health. This question is important in quiescent NSCs, which are the head of the neural lineage, and present throughout life.

B) Quiescent NSCs directly isolated from the SVZ exhibit less protein synthesis than their activated counterparts. Protein synthesis is measured by acutely incubating the 4 SVZ populations directly FACS-sorted from the SVZ with OP-puromycin (OPP), which is incorporated into nascent proteins. OPP levels are measured by fluorescent click-chemistry detection followed by flow cytometry. Y-axis represents the median OPP fluorescence of each cell population, normalized to cell size (forward scatter), and normalized to the median OPP/forward scatter value on the day of measurement. Each point represents FACS-sorted cells from a single mouse. Bars represent mean -/+ sem of values from 4 different mice (3-4 months old) analyzed on 2 different days. p-value was calculated using the one-sided Wilcoxon rank-sum test. * $p \leq 0.05$.

C) Schematic illustration of the experimental design for biochemical fractionation of protein aggregates. Two thirds of each sample was lysed using standard RIPA buffer to dissolve soluble proteins ('soluble fraction') and the remaining insoluble protein pellet ('insoluble fraction', enriched in protein aggregates) was solubilized in a 4% SDS buffer. One third of each sample was solubilized directly in 4% SDS buffer and used for normalization ('total fraction').

D) Quantification of overall protein insolubility in qNSC and aNSC primary cultures. The Y-axis represents the raw intensity density of each insoluble fraction gel lane (entire lane) normalized to the raw intensity density of the corresponding total fraction gel lane (entire lane), quantified by Fiji. Each point represents one independent primary culture derived from two 3-4-month-old mice. Bars represent mean -/+ sem of values from 3 primary cultures. p-values were calculated using the one-sided Wilcoxon rank-sum test. * $p \leq 0.05$.

E) Quantification of high molecular weight aggregates in qNSC and aNSC primary cultures. The Y-axis represents the raw intensity density of each "SDS-resistant" high molecular weight band (protein that did not migrate into the gel; see Fig. 2C) normalized to the raw intensity density of the corresponding total fraction gel lane (entire lane), quantified by Fiji. High molecular weight complexes that do not migrate into the gel are characteristic of highly ordered amyloid-like aggregates, which are SDS-resistant and therefore too large to migrate through the gel (*22*). Each point represents one independent primary culture from two 3-4-month-old mice. Bars represent mean -/+ sem of values from 3 independent primary cultures. p-values were calculated using the one-sided Wilcoxon rank-sum test. * $p \leq 0.05$.

Fig. S7. Nutrient deprivation and TFEB expression in qNSCs

A) Quiescent NSC primary cultures were treated with DMSO or 50 nm Bafilomycin A (BafA; to deacidify lysosomes) for 18 hours, stained with Lamp-2 antibody, and analyzed by intracellular flow cytometry. The Y-axis represents the median fluorescence of Lamp-2 of each sample normalized to the median value per replicate (to combine samples run at different times). Each point represents one independent primary culture derived from two 3-4-month-old mice. Mean -/+ sem of values from 6 biological replicates analyzed on two different days. p-values calculated using the one-sided Wilcoxon rank-sum test. ** $p \leq 0.01$.

B) Quantification of lysosomal area after nutrient deprivation of primary cultures of qNSCs. Differences in Lamp-2^{+} area quantified indicate a statistically significant difference between qNSC primary cultures under basal conditions compared to those

subjected to a 3 hour pulse of nutrient deprivation in Hank's Balanced Salt Solution (HBSS). Each point represents one independent primary culture derived from two 3-4-month-old mice. Bars represent mean -/+ sem of values from 8 primary cultures from 3 independent experiments. Note that the qNSC data are also shown in Fig. S5B. p-values were calculated using the one-sided Wilcoxon rank-sum test. * $p \leq 0.05$.

C) Representative SDS-PAGE gel stained with SYPRO Ruby for detection of protein in the total and insoluble fractions of qNSC primary cultures under basal conditions or subjected to nutrient deprivation for 3 hours in Hank's Balanced Salt Solution (HBSS). High molecular weight complexes that do not migrate into the gel are characteristic of highly ordered amyloid-like aggregates, which are SDS-resistant and therefore too large to migrate through the gel (*22*). A short exposure of the film is shown in order to best display the differences in the in high molecular weight fraction between basal and nutrient deprivation conditions. Samples are derived from young adult (Y; 3-month)) or old (O; 20-month) qNSC primary cultures.

D) Nutrient deprivation leads to a reduction in the overall insoluble fraction of qNSCs. Left panel: Quantification of overall protein insolubility in young adult qNSC primary cultures. The Y-axis represents the raw intensity density of each insoluble fraction gel lane (entire lane) normalized to the raw intensity density of the corresponding total fraction gel lane (entire lane), quantified by Fiji. Each point represents one independent primary culture derived from two 3-4-month-old mice. Bars represent mean -/+ sem of values from 3 independent primary cultures. p-values were calculated using the one-sided Wilcoxon rank-sum test. * $p \leq 0.05$. Right panel: Biochemical fractionation by protein solubility reveals a reduction in high-molecular weight insoluble proteins (SDS-resistant

protein aggregates) in response to nutrient deprivation. Quantification of high molecular weight insoluble aggregates in qNSCs. The Y-axis represents the raw intensity density of each "SDS-resistant" high molecular weight band (protein that did not migrate into the gel; see Fig. S7C) normalized to the raw intensity density of the corresponding total fraction gel lane (entire lane), quantified by Fiji. To compare gels run on different days, all values are additionally normalized to the median fluorescence value on their day of analysis. Each point represents one independent primary culture derived from two 3-4-month-old mice. Bars represent mean -/+ sem of values from 3 independent primary cultures. p-values were calculated using the one-sided Wilcoxon rank-sum test. * $p \leq 0.05$.

E) Differential effect of nutrient deprivation on qNSCs, qNSCs responding to activation growth factors, and aNSCs. Left panel: Nutrient deprivation in qNSCs does not induce proliferation in the absence of activating growth factors. Primary cultures of qNSCs were incubated in basal quiescence medium or in Hank's Balanced Salt Solution (HBSS) containing EdU for 1 hour. Proliferation (determined by the percentage of cells positive for EdU, which is incorporated into newly synthesized DNA during S-phase) was then measured by fluorescent click-chemistry detection followed by intracellular flow cytometry. Middle and right panels: Nutrient deprivation in aNSCs reduces proliferation whereas nutrient deprivation in qNSCs increases their activation in response to growth factors. Primary cultures of qNSCs and aNSCs were subjected to a 1-hour pulse of nutrient deprivation in Hank's Balanced Salt Solution (HBSS) and both where then cultured in activation medium containing growth factors for 8 days. Proliferation was then measured by incubating cells for 3 hours with EdU and performing fluorescent

click-chemistry detection followed by intracellular flow cytometry. The Y-axes represent the percentage of cells in an individual culture that incorporated EdU. Each point represents one independent primary culture derived from two 3-4-month-old mice. Bars represent mean -/+ sem of values from 3 different biological replicates analyzed on a single day. p-values were calculated using the one-sided Wilcoxon rank-sum test. * $p \leq 0.05$.

F) Expression of TFEB and TFEB target genes in qNSCs. Young qNSCs were infected with lentiviruses expressing a doxycyclin-inducible form of constitutively active TFEB and rtTA, or rtTA alone as control. After two days, cells were treated for 48 hours doxycyclin and total RNA was extracted. RT-qPCR was performed on known TFEB target genes. Labels below the X-axis indicate a subset of TFEB target genes that are significantly more highly expressed in aNSCs in the brain (based on RNA-seq), and were analyzed here in qNSCs for differential expression after 48 hours of TFEB induction. TFEB target genes are color-coded by their main function. Results were normalized to the average of three house-keeping genes (*Hprt*, *Gapdh*, and *actin*) and analyzed using the ΔΔ-CT method. p-values were calculated using a two-sided t-test. **** $p \leq 0.0001$, ** $p \leq 0.01$, * $p \leq 0.05$.

Fig. S8. RNA-seq analysis of global age-dependent differences between neural lineage cell types

A) Quiescent neural lineage populations (qNSCs, astrocytes) show higher absolute expression fold changes with age genome-wide compared to activated neural lineage populations (aNSCs, NPCs). Shown are the distributions of the absolute log2 fold

changes between young and old of all detected genes for each cell type, based on differential expression analysis using DESeq2. The medians of the log2 fold changes of genes with age in qNSCs and aNSCs are significantly different using the Wilcoxon rank-sum test ("sig": p-value < 10e-100; it should be noted that the strong significance is due in part to the observations for this test being 15,329 genes).

B) Distributions of gene-wise coefficients of variance (CV) across all samples of the same cell type and age group, based on VST-normalized read counts of all detected genes, accounting for the day of FACS.

C) Differential expression analysis between young and old detects more differentially expressed genes with age in quiescent than in activated neural lineage populations. Shown are the log2 fold changes between young and old of each cell type for all detected genes, based on differential expression analysis using an alternative pipeline (SVA/limma). Each point represents one gene. Genes in color are significantly up- or down-regulated with age ("sig.") with FDR = 0.05. Genes in grey are not significantly up- or down-regulated with age.

D) Quiescent neural lineage populations show increased absolute expression fold changes with age genome-wide compared to activated neural lineage populations. Shown are the distributions of the absolute log2 fold changes between young and old of all detected genes for each cell type, based on differential expression analysis using an alternative pipeline (SVA/limma). The distributions of the log2 fold changes of genes with age in qNSCs and aNSCs are significantly different using the Wilcoxon rank-sum test ("sig": p-value < 10e-100; it should be noted that the strong significance is due in part to the observations for this test being 14,330 genes rather than independent biological samples).

E) PCA separates between young and old endothelial cells, and young and old quiescent neural lineage populations, but not young and old activated neural lineage populations. PCA of endothelial cells, the 2 quiescent neural lineage populations, and the two activated neural lineage populations (from left to right), based on VST-normalized read counts of all detected genes, taking into account the day of FACS.

F) Principal component analysis (PCA) of the young and old transcriptomes of each cell type using an alternative pipeline based on surrogate variable analysis (SVA) and limma (see Materials and Methods for details). PCA separates between young and old transcriptomes of endothelial cells (Endo) and quiescent neural lineage populations (astrocytes and quiescent neural stem cells), but not young and old activated neural lineage populations (activated neural stem cells and neural progenitor cells). PCAs are based on log2-transformed FPKM values of TMM-normalized read counts of all detected genes, accounting for surrogate variables.

G) The KEGG lysosome pathway is significantly upregulated in qNSCs with age (FDR-adjusted $p \leq 0.05$). The average log2 fold change with age of the KEGG lysosome and proteasome pathways in qNSCs and aNSCs directly FACS sorted from the brain are plotted. Targeted evaluation of these two KEGG pathways was performed by calculating the arithmetic mean of gene-wise test statistics (Wald test statistic from differential expression analysis between young and old using DESeq2) per pathway. p-values were obtained by bootstrap sampling and corrected for multiple hypothesis testing of the proteasome and lysosome pathways (using the Benjamini-Hochberg algorithm).

Fig. S9. Changes in lysosomes and protein aggregates with age in qNSCs and aNSCs

A) Lysosome levels in primary cultures of qNSCs and aNSCs from young adult and old mice. Cells were stained with Lamp-2 antibody and analyzed by intracellular flow cytometry. The Y-axis represents the median fluorescence value of each sample normalized to the median qNSC value per replicate (to combine samples run at different times). Each point represents one independent primary culture derived from two 3-4-month-old mice or two 17-20-month-old mice. Mean -/+ sem of values from 6 biological replicates analyzed on two different days. p-values calculated using the one-sided Wilcoxon rank-sum test. ** $p \leq 0.01$.

B) LysoTracker Red levels in young and old primary cultured qNSCs and aNSCs. Live cells were stained with LysoTracker Red and analyzed by intracellular flow cytometry. As a control for specificity, young qNSCs (Q) and aNSCs (A) were also treated with 400 nM Bafilomycin A (BafA) for 2 hours to inhibit lysosomal acidification. The Y-axis represents the median LysoTracker Red fluorescence value of each sample. Each point represents one independent primary culture derived from two 3-4-month-old mice or two 20-month-old mice. Mean -/+ sem of values from 3 biological replicates analyzed on a single day. p-value calculated using the one-sided Wilcoxon rank-sum test. * $p \leq 0.05$.

C) Quantification of GFP-LC3 levels in young and old qNSCs and aNSCs shows that a subset of old qNSCs exhibit elevated levels of GFP-LC3. Populations of qNSCs and aNSCs/NPCs were isolated from GFP-LC3 transgenic mice and the level of GFP fluorescence was assessed. High GFP-LC3 fluorescence is indicative of an accumulation of LC3/autophagosomes that have not fused with an acidified lysosome. The Y-axis represents the fluorescence of GFP-LC3 normalized to cell size and to the median young value on the day of measurement to combine independent experiments. The 5^{th}, 50^{th}

(median), and 95th percentiles are plotted for each mouse analyzed. Each point represents FACS-sorted cells from a single mouse. Bars represent mean -/+ sem of values from 18 young mice (2-5 months old) and 13 old mice (25-28 months old) analyzed on 4 different days. p-values: two-sided Wilcoxon rank-sum test. **** $p \leq 0.0001$, * $p \leq 0.05$. Representative histogram shown in Fig. 4D.

D) Increased heterogeneity with age in levels of LC3/autophagosomes outside of lysosomes. Left panel: Violin plots of single-cell GFP-LC3 fluorescence across the quiescent NSC populations from 18 young (2-5 month-old) and 13 old (25-28 month-old) GFP-LC3 mice analyzed on 4 different days (same data as in Fig. S9C). The Y-axis represents the logged fluorescence of GFP-LC3 normalized to the median value on the day of measurement to combine independent experiments. Note the upper 'bulge' in the violin plot for old qNSCs – a characteristic of a heterogeneous population. Right panel: Heterogeneity of GFP-LC3 in old qNSCs. The Y-axis represents the median absolute deviation of log GFP-LC3 fluorescence normalized to the median value on the day of measurement to combine independent experiments. Each point represents FACS-sorted cells from a single mouse. Bars represent mean -/+ sem of values from 18 young mice (2-5 months old) and 13 old mice (25-28 months old) analyzed on 4 different days (same data as in Fig. S9C). p-values: one-sided Wilcoxon rank-sum test. ** $p \leq 0.01$.

E) Level of catalytically active proteasomes in quiescent and activated populations directly isolated from the SVZ do not change significantly with age. The level of catalytically active proteasomes is measured by acutely staining mixed Ast/qNSC populations or mixed aNSC/NPC populations directly FACS-sorted from the brain of young adult and old mice with Me4BodipyFL-Ahx3Leu3VS, which covalently binds

active proteasomes (populations are mixed because GFAP-GFP mice could not be used in combination with the green fluorescence of Me4BodipyFL-Ahx3Leu3VS. See Materials and Methods for details). The Y-axis represents the proteasome-specific fluorescence value of each population calculated as the median Me4BodipyFL-Ahx3Leu3VS fluorescence minus non-specific fluorescence determined by pre-treating half of each sample in parallel with the proteasome inhibitor MG132. Each point represents either the Ast/qNSC or the aNSC/NPC cells FACS-sorted from a single young adult (3-4 month) or a single old mouse (24-month). Note that the data from young mice are also shown in Fig. 1I. Bars represent mean -/+ sem of values from 3-4 different mice analyzed on two different experimental days.

F) Aggregate levels in primary cultures of qNSCs and aNSCs from young adult and old mice. Cells were stained with Proteostat and analyzed by intracellular flow cytometry. The Y-axis represents the median fluorescence value of each sample normalized to the median qNSC value per replicate (to combine samples run at different times). Each point represents one independent primary culture derived from two 3-4-month-old mice or two 17-20-month-old mice. Mean -/+ sem of values from 9 biological replicates analyzed on three different days. p-values calculated using the one-sided Wilcoxon rank-sum test. *** $p \leq 0.001$.

G) The subpopulation of aged qNSCs with high levels of autophagosomes and protein aggregates is reduced after 48 hours of fasting. Old (21-month-old) GFP-LC3 mice were subjected to 48 hours of fasting or allowed to eat *ad libitum*. Left panel: representative histograms of GFP-LC3 expression in qNSCs from old fasted or *ad libitum* GFP-LC3 mice. Middle panel: Frequency of GFP-LC3-high cells in the starved vs. *ad libitum* old

GFP-LC3 qNSC population. The cutoff for GFP-high cells was set for each pair of fasted and *ad libitum* mice at the local minimum between the GFP-high and GFP-low sides of the bimodal histogram of the *ad libitum* mouse. Each point represents one mouse. Mean -/+ sem of values from 4 biological replicates analyzed on a single day. p-values calculated using the one-sided Wilcoxon rank-sum test. * $p \leq 0.05$. Right panel: Proteostat level in GFP-high qNSCs (top 40%) sorted from the SVZs of GFP-LC3 fasted or *ad libitum* mice. The Y-axis represents the median fluorescence of Proteostat normalized to the median Proteostat value per replicate (to combine samples processed at different times). Each point represents one 21-month-old mouse. Mean -/+ sem of values from 4 biological replicates analyzed on a single day. p-values calculated using the one-sided Wilcoxon rank-sum test. * $p \leq 0.05$.

H) Collectively, our results suggest that in young adult qNSCs, degradation of the abundant aggregate-filled lysosomes enhances qNSC ability to respond to activation signals. In old qNSCs, abundance of these lysosomes is reduced, which is linked with an accumulation of aggregates and autophagosomes that have not yet fused with lysosomes, as well as a reduced ability to respond to activation signals. However, dietary or genetic manipulations enhancing the lysosome-autophagy pathway can reduce aggregates and rejuvenate the ability of old qNSCs to respond to activation signals.

Figure S1

A FACS scheme to isolate 5 different cell types from the SVZs of young and old GFAP-GFP transgenic mice

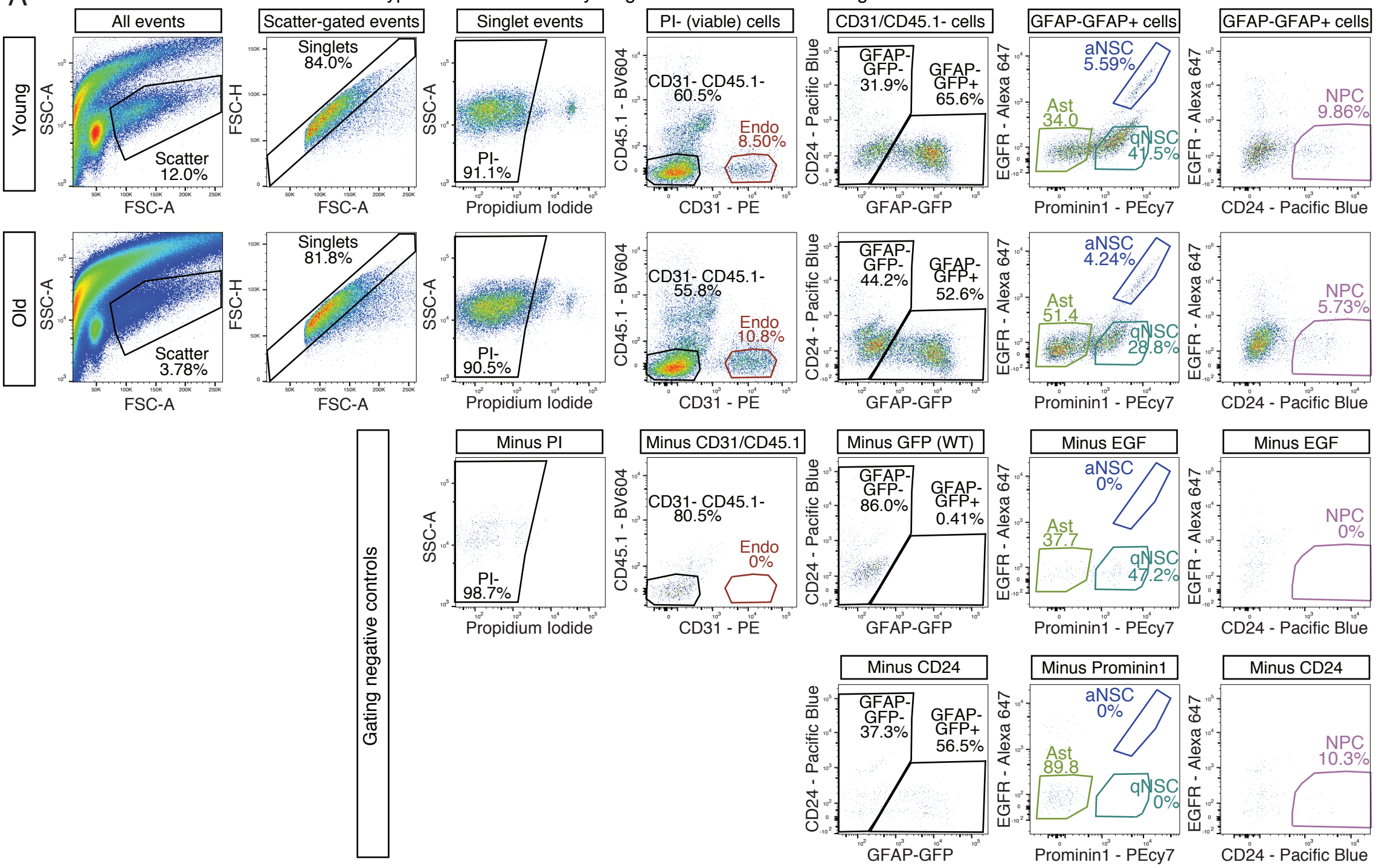

B

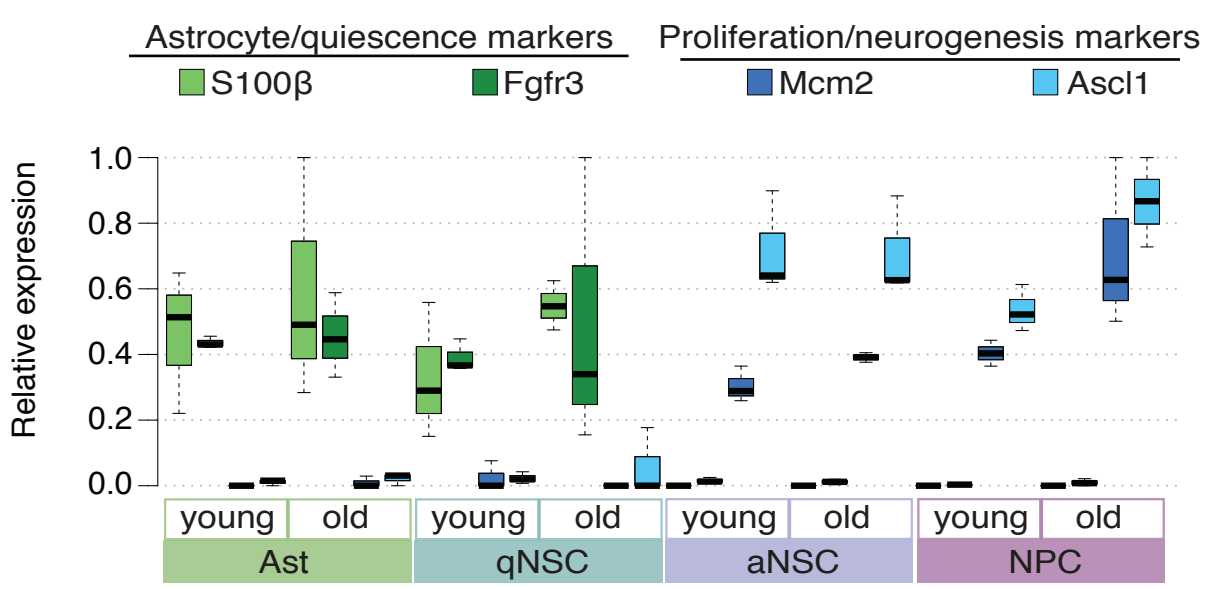

C

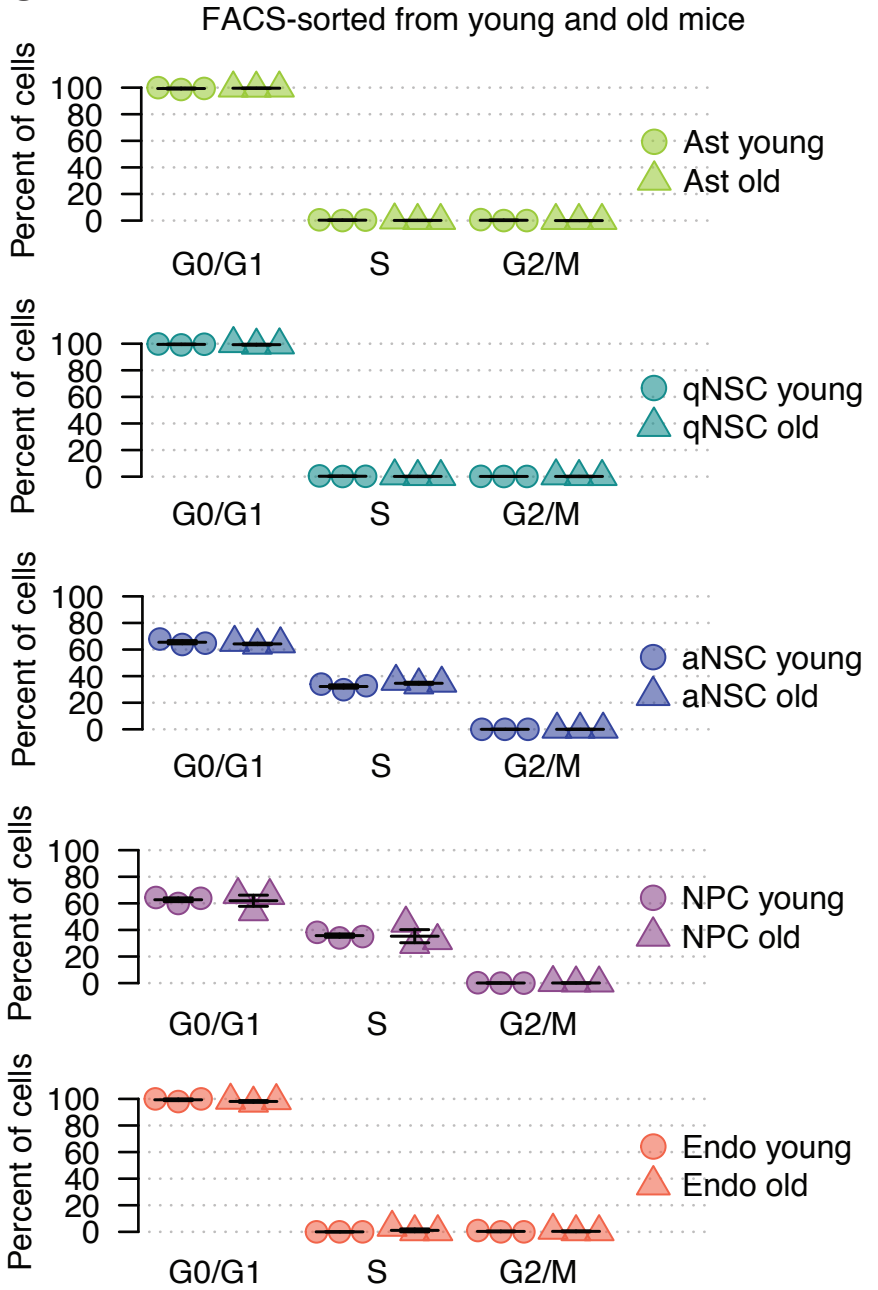

Figure S2

A Absence of batch effect from sequencing lane

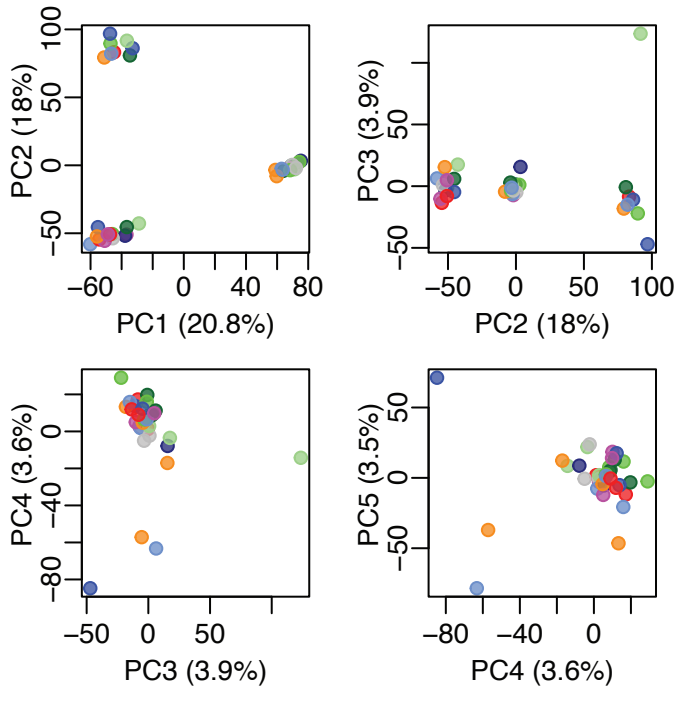

B Subtle batch effect from day of FACS

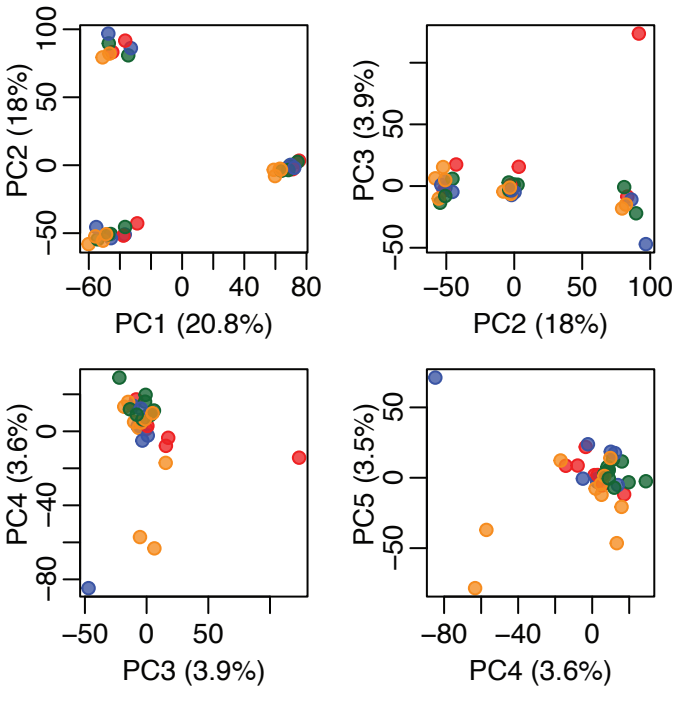

C Expression of astrocyte and quiescence markers (RNA-seq)

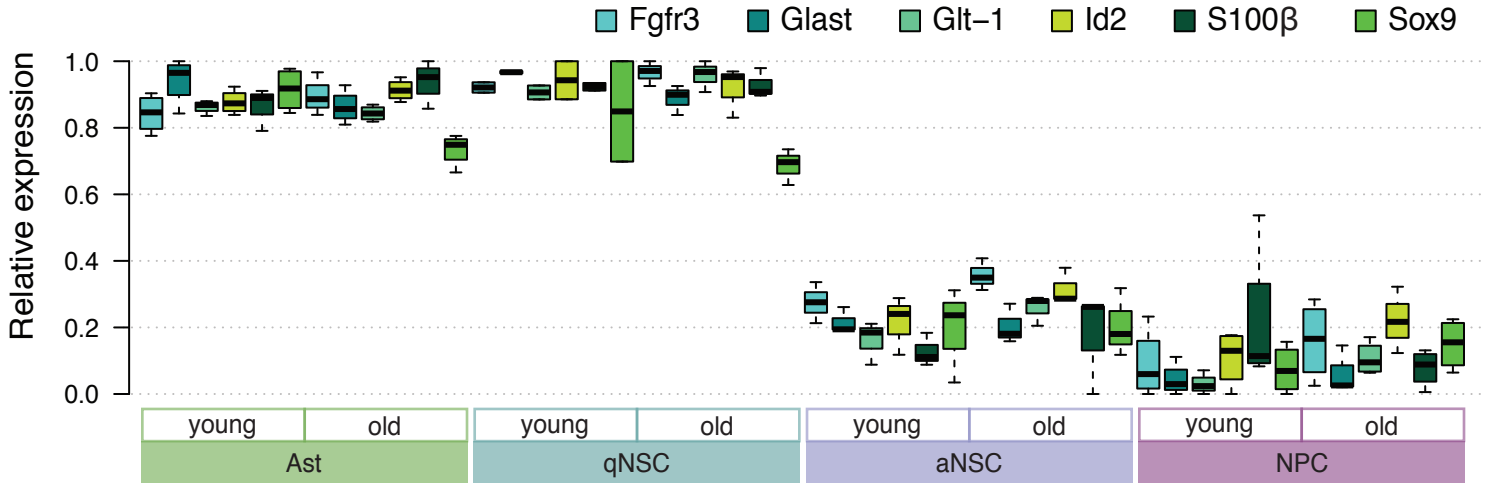

Expression of proliferation and neurogenesis markers (RNA-seq)

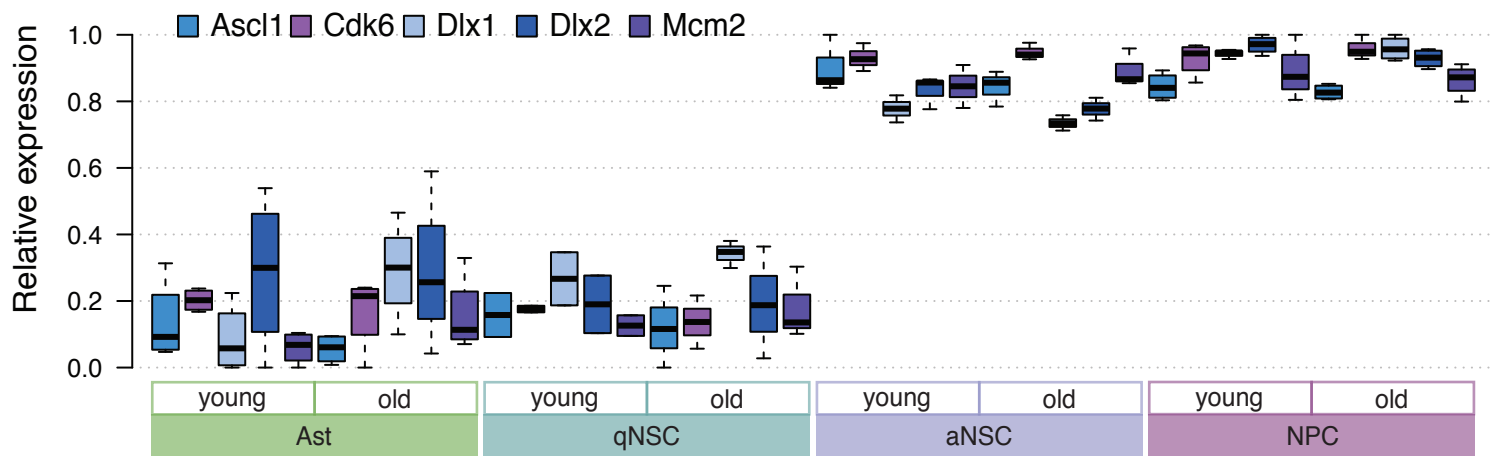

Expression of endothelial and hematopoietic markers (RNA-seq)

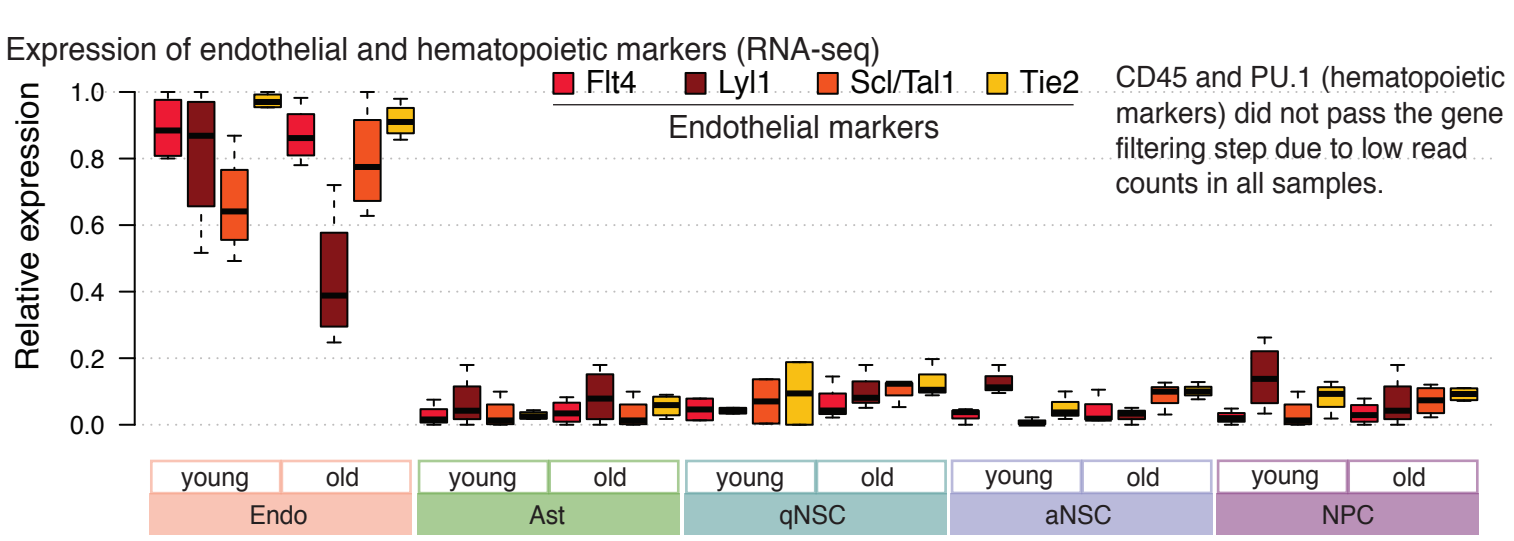

CD45 and PU.1 (hematopoietic markers) did not pass the gene filtering step due to low read counts in all samples.

D

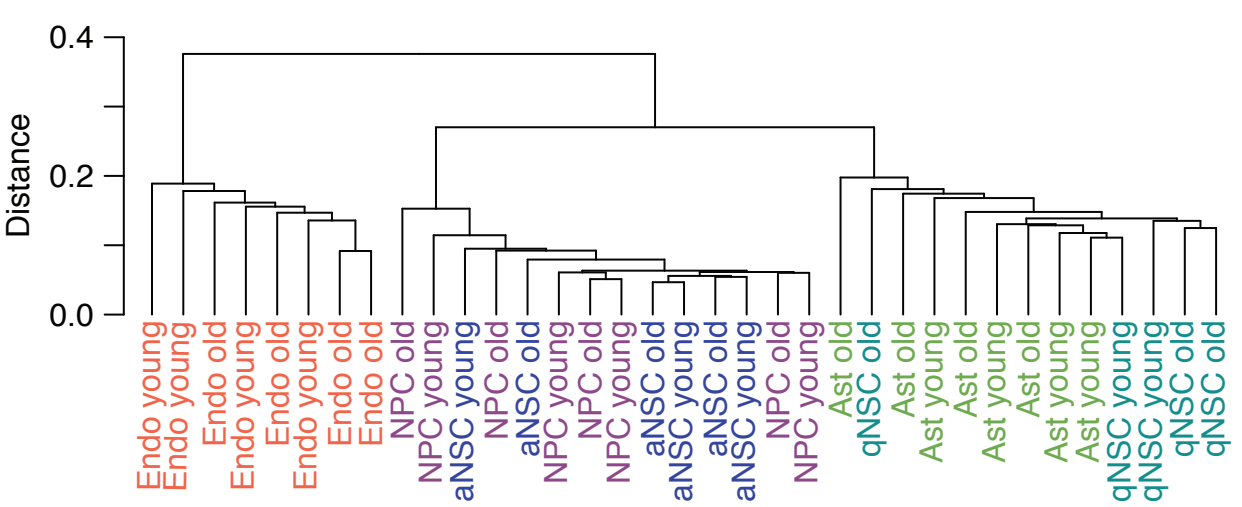

Figure S3

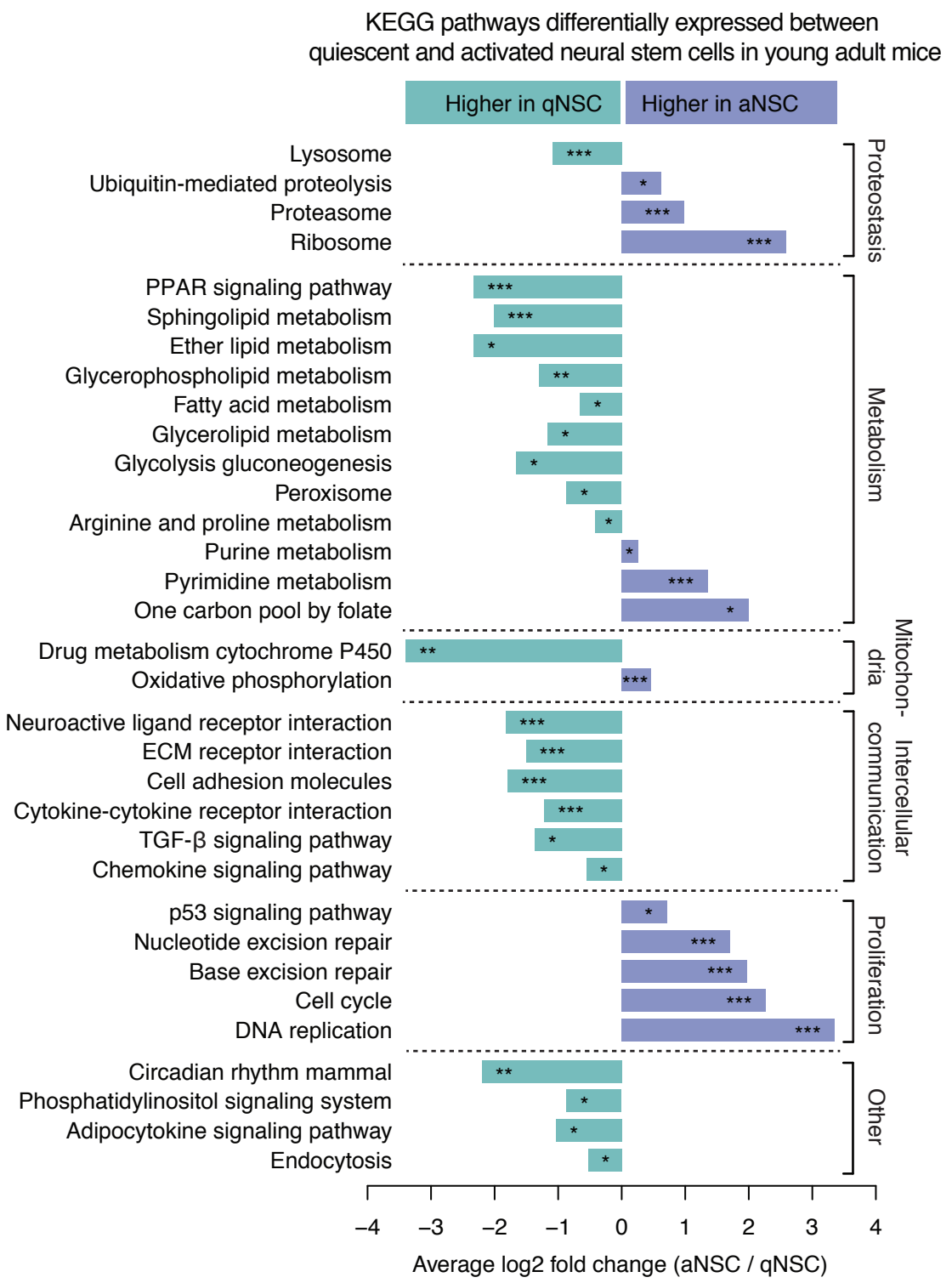
A
KEGG pathways differentially expressed between quiescent and activated neural stem cells in young adult mice
Higher in qNSC
Higher in aNSC
Lysosome
Ubiquitin-mediated proteolysis
Proteasome
Ribosome
PPAR signaling pathway
Sphingolipid metabolism
Ether lipid metabolism
Glycerophospholipid metabolism
Fatty acid metabolism
Glycerolipid metabolism
Glycolysis gluconeogenesis
Peroxisome
Arginine and proline metabolism
Purine metabolism
Pyrimidine metabolism
One carbon pool by folate
Drug metabolism cytochrome P450
Oxidative phosphorylation
Neuroactive ligand receptor interaction
ECM receptor interaction
Cell adhesion molecules
Cytokine-cytokine receptor interaction
TGF-β signaling pathway
Chemokine signaling pathway
p53 signaling pathway
Nucleotide excision repair
Base excision repair
Cell cycle
DNA replication
Circadian rhythm mammal
Phosphatidylinositol signaling system
Adipocytokine signaling pathway
Endocytosis
Proteostasis
Metabolism
Mitochon-dria
Intercellular communication
Proliferation
Other
−4 −3 −2 −1 0 1 2 3 4
Average log2 fold change (aNSC / qNSC)

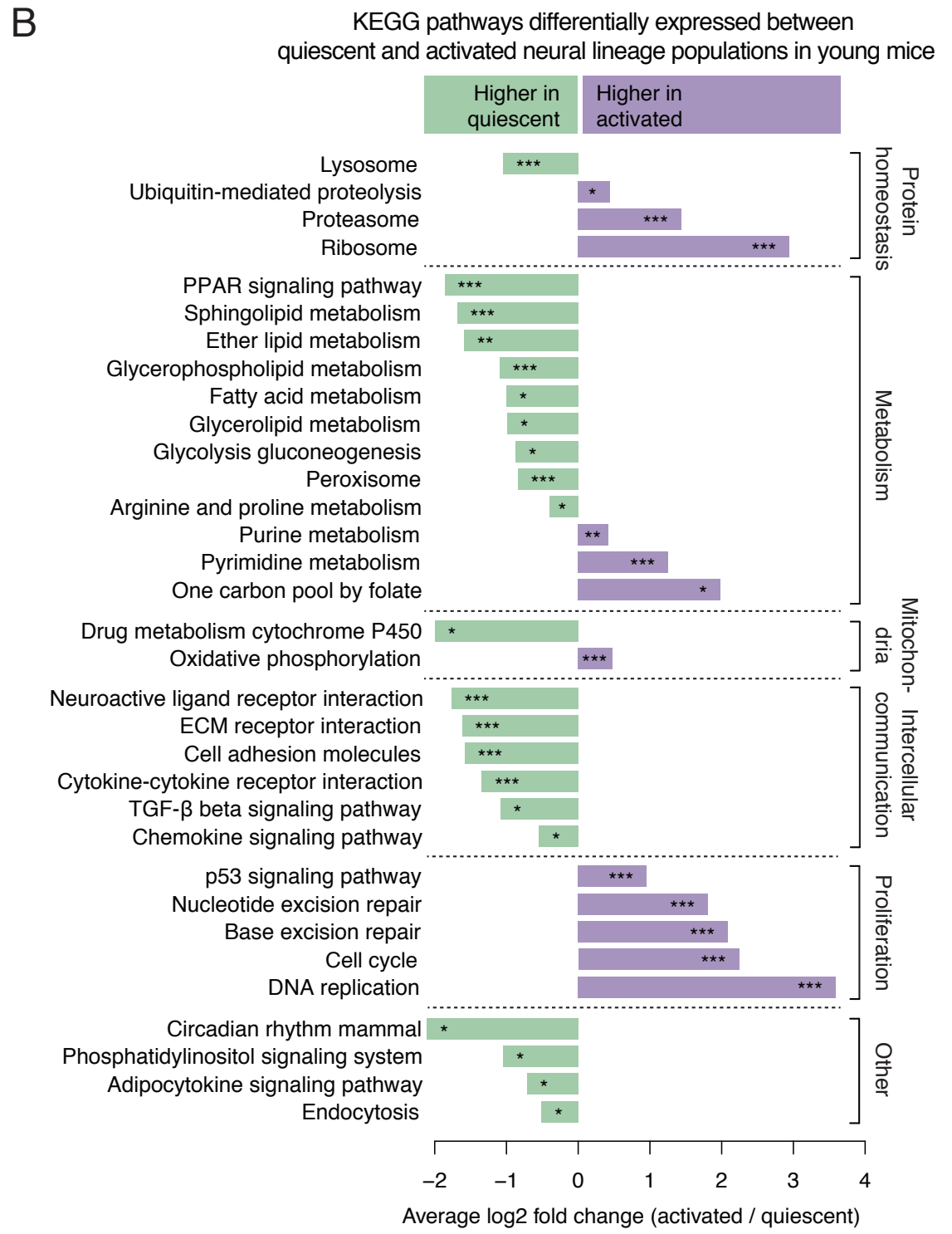
B
KEGG pathways differentially expressed between quiescent and activated neural lineage populations in young mice
Higher in quiescent
Higher in activated
Lysosome
Ubiquitin-mediated proteolysis
Proteasome
Ribosome
PPAR signaling pathway
Sphingolipid metabolism
Ether lipid metabolism
Glycerophospholipid metabolism
Fatty acid metabolism
Glycerolipid metabolism
Glycolysis gluconeogenesis
Peroxisome
Arginine and proline metabolism
Purine metabolism
Pyrimidine metabolism
One carbon pool by folate
Drug metabolism cytochrome P450
Oxidative phosphorylation
Neuroactive ligand receptor interaction
ECM receptor interaction
Cell adhesion molecules
Cytokine-cytokine receptor interaction
TGF-β beta signaling pathway
Chemokine signaling pathway
p53 signaling pathway
Nucleotide excision repair
Base excision repair
Cell cycle
DNA replication
Circadian rhythm mammal
Phosphatidylinositol signaling system
Adipocytokine signaling pathway
Endocytosis
Protein homeostasis
Metabolism
Mitochon-dria
Intercellular communication
Proliferation
Other
−2 −1 0 1 2 3 4
Average log2 fold change (activated / quiescent)

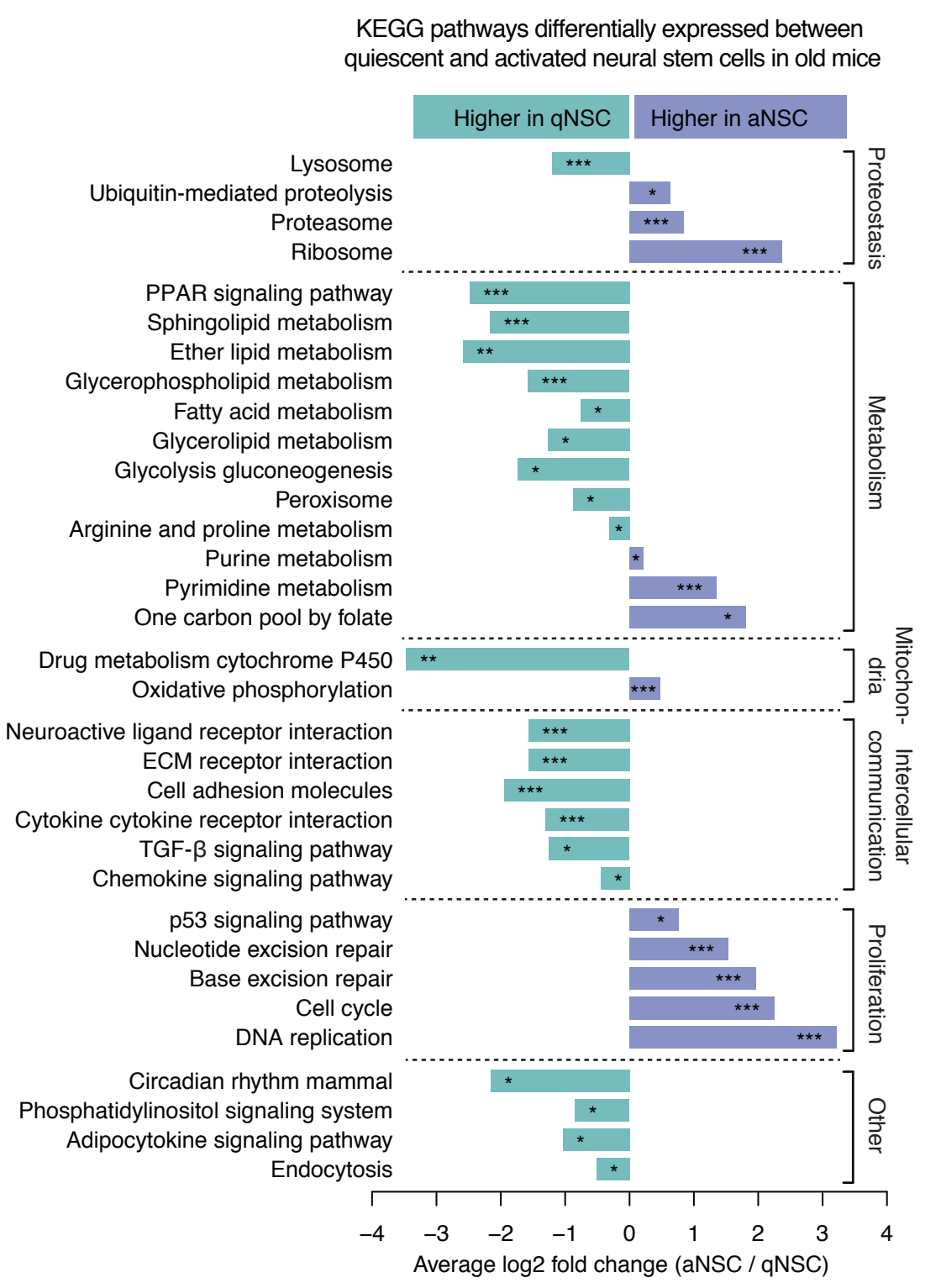
C
KEGG pathways differentially expressed between quiescent and activated neural stem cells in old mice
Higher in qNSC
Higher in aNSC
Lysosome
Ubiquitin-mediated proteolysis
Proteasome
Ribosome
PPAR signaling pathway
Sphingolipid metabolism
Ether lipid metabolism
Glycerophospholipid metabolism
Fatty acid metabolism
Glycerolipid metabolism
Glycolysis gluconeogenesis
Peroxisome
Arginine and proline metabolism
Purine metabolism
Pyrimidine metabolism
One carbon pool by folate
Drug metabolism cytochrome P450
Oxidative phosphorylation
Neuroactive ligand receptor interaction
ECM receptor interaction
Cell adhesion molecules
Cytokine cytokine receptor interaction
TGF-β signaling pathway
Chemokine signaling pathway
p53 signaling pathway
Nucleotide excision repair
Base excision repair
Cell cycle
DNA replication
Circadian rhythm mammal
Phosphatidylinositol signaling system
Adipocytokine signaling pathway
Endocytosis
Proteostasis
Metabolism
Mitochon-dria
Intercellular communication
Proliferation
Other
−4 −3 −2 −1 0 1 2 3 4
Average log2 fold change (aNSC / qNSC)

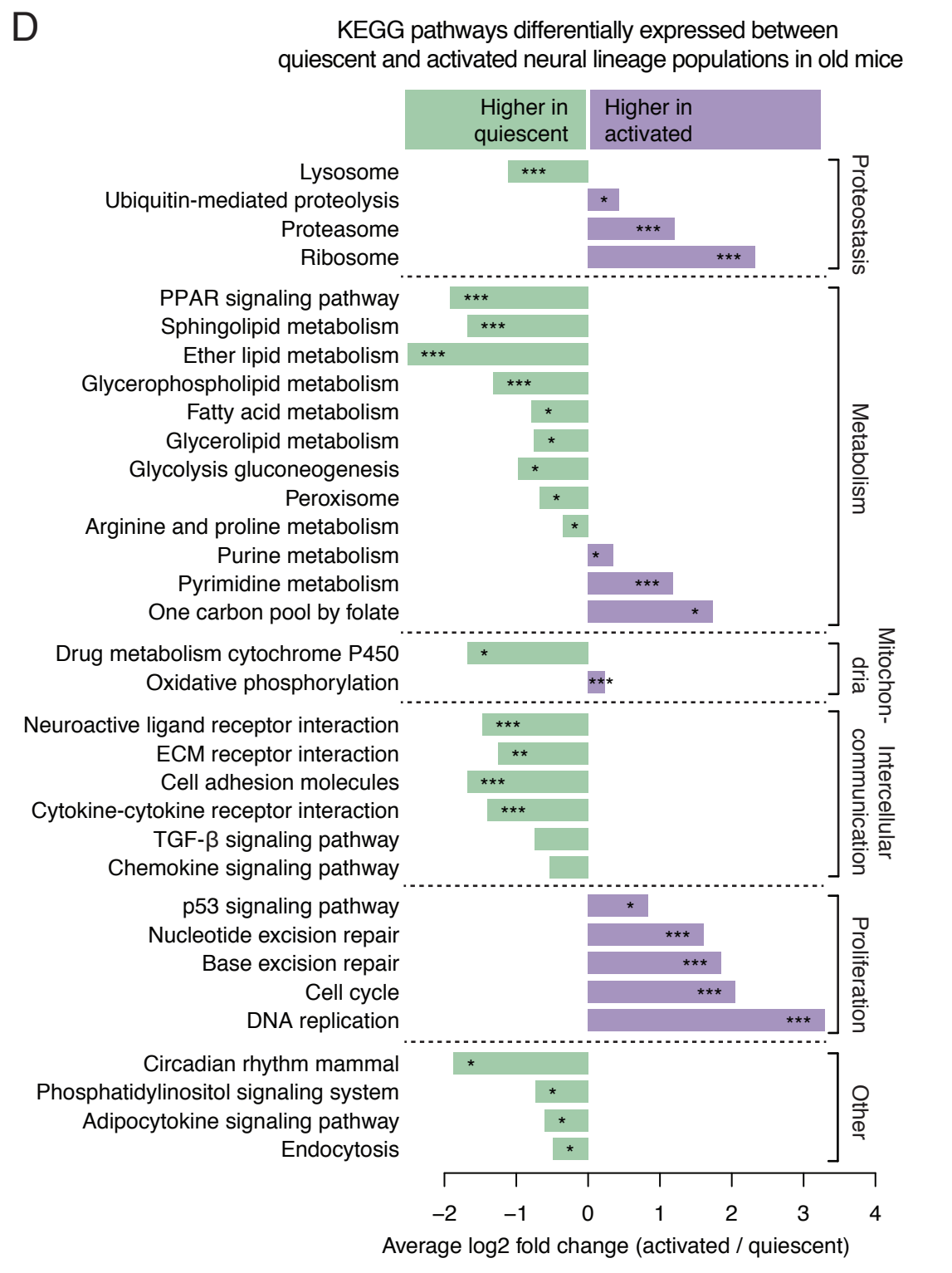
D
KEGG pathways differentially expressed between quiescent and activated neural lineage populations in old mice
Higher in quiescent
Higher in activated
Lysosome
Ubiquitin-mediated proteolysis
Proteasome
Ribosome
PPAR signaling pathway
Sphingolipid metabolism
Ether lipid metabolism
Glycerophospholipid metabolism
Fatty acid metabolism
Glycerolipid metabolism
Glycolysis gluconeogenesis
Peroxisome
Arginine and proline metabolism
Purine metabolism
Pyrimidine metabolism
One carbon pool by folate
Drug metabolism cytochrome P450
Oxidative phosphorylation
Neuroactive ligand receptor interaction
ECM receptor interaction
Cell adhesion molecules
Cytokine-cytokine receptor interaction
TGF-β signaling pathway
Chemokine signaling pathway
p53 signaling pathway
Nucleotide excision repair
Base excision repair
Cell cycle
DNA replication
Circadian rhythm mammal
Phosphatidylinositol signaling system
Adipocytokine signaling pathway
Endocytosis
Proteostasis
Metabolism
Mitochon-dria
Intercellular communication
Proliferation
Other
−2 −1 0 1 2 3 4
Average log2 fold change (activated / quiescent)

Figure S4

A

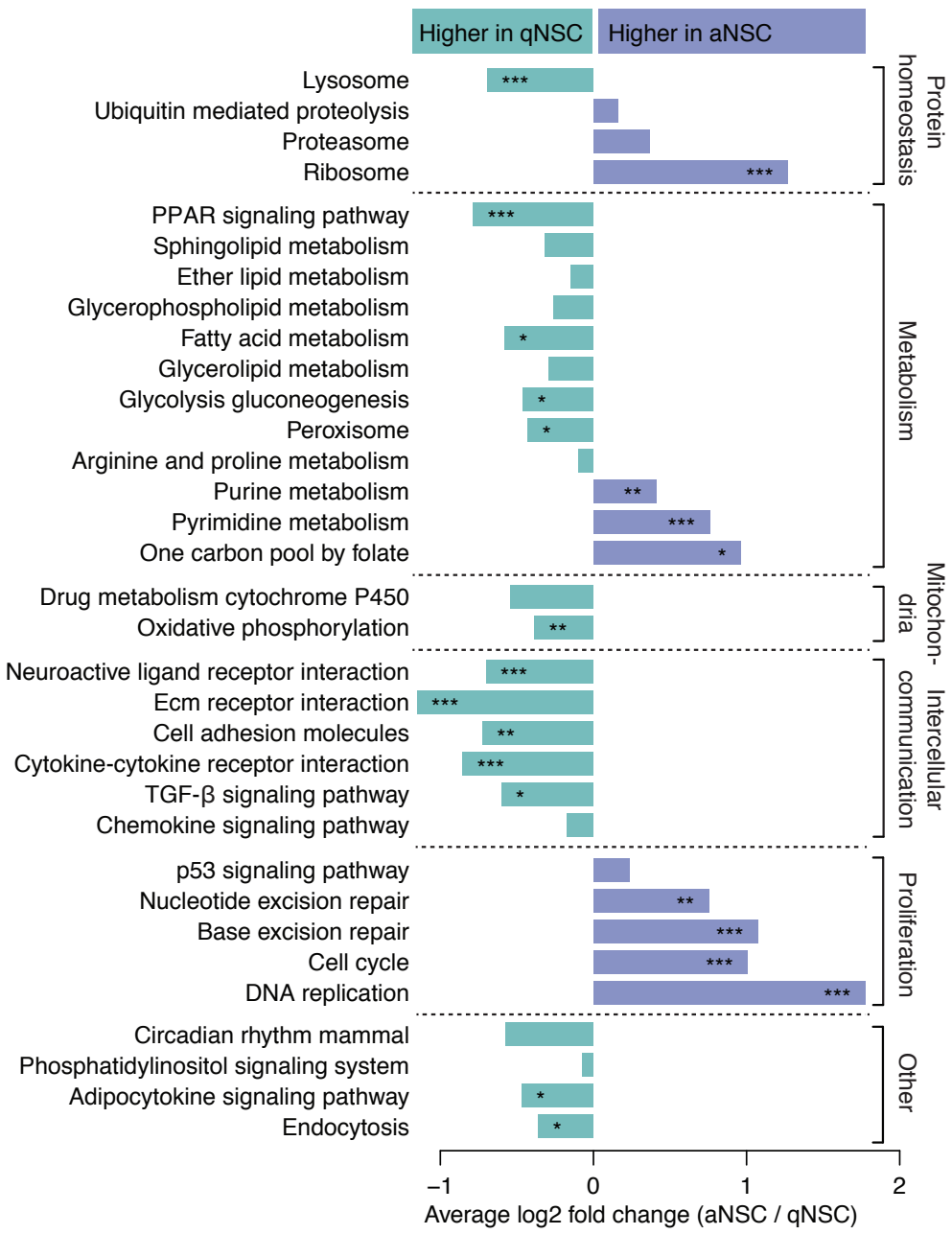

B

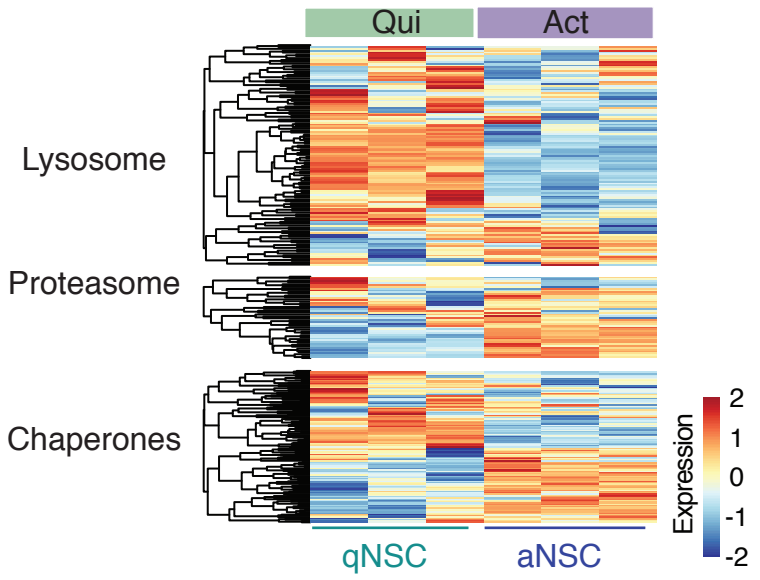

C

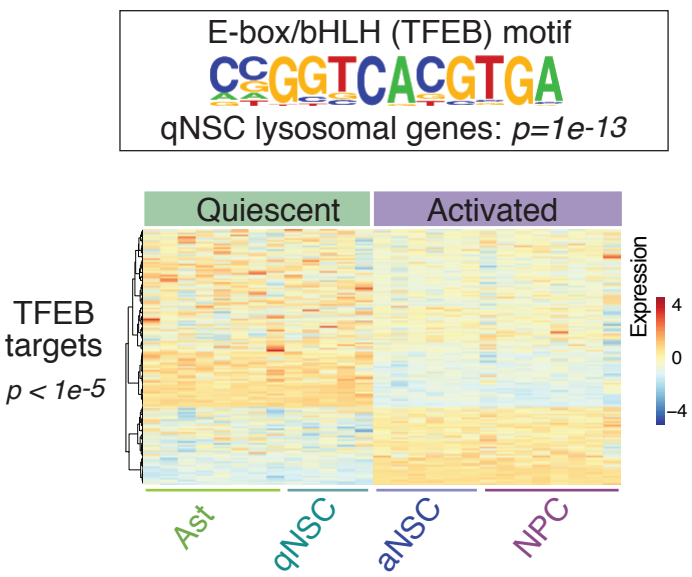

D

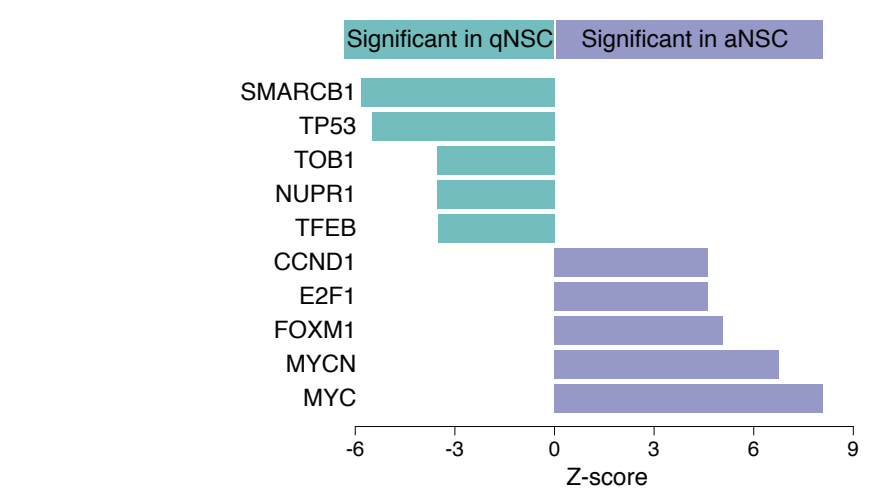

E

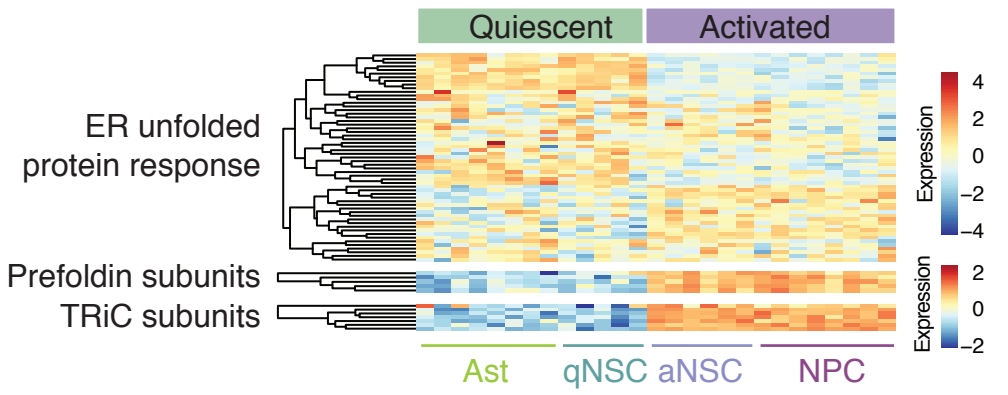

F

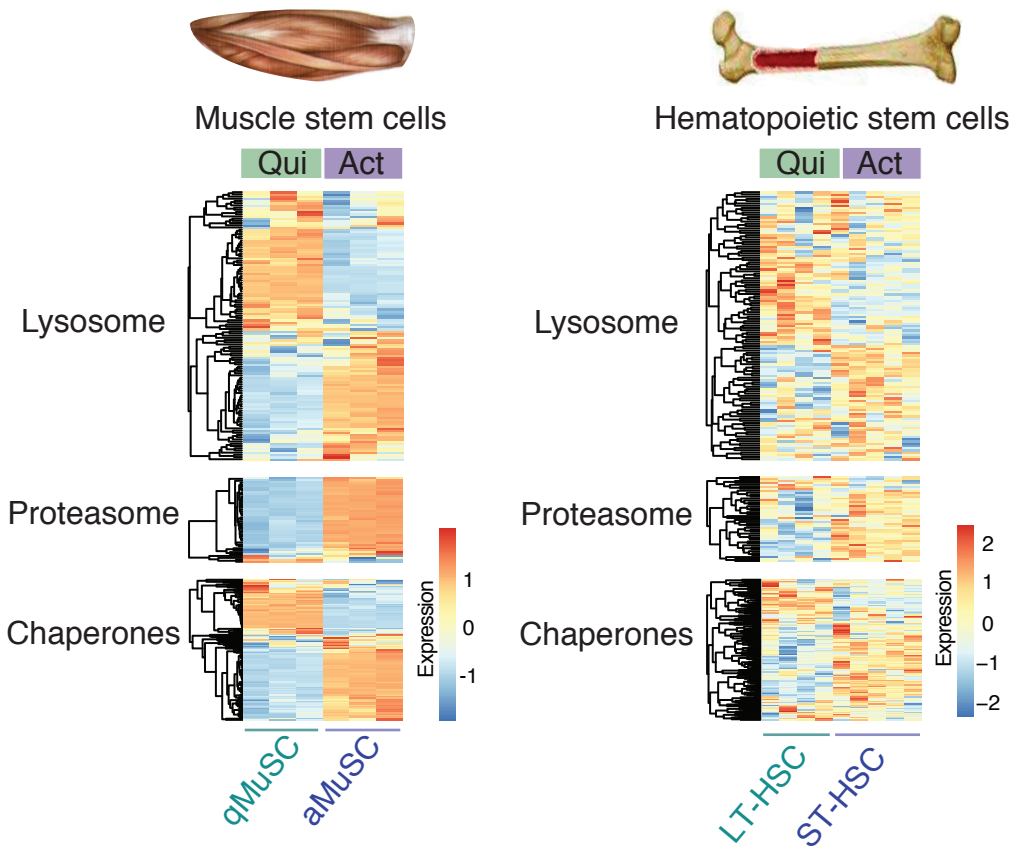

Figure S5

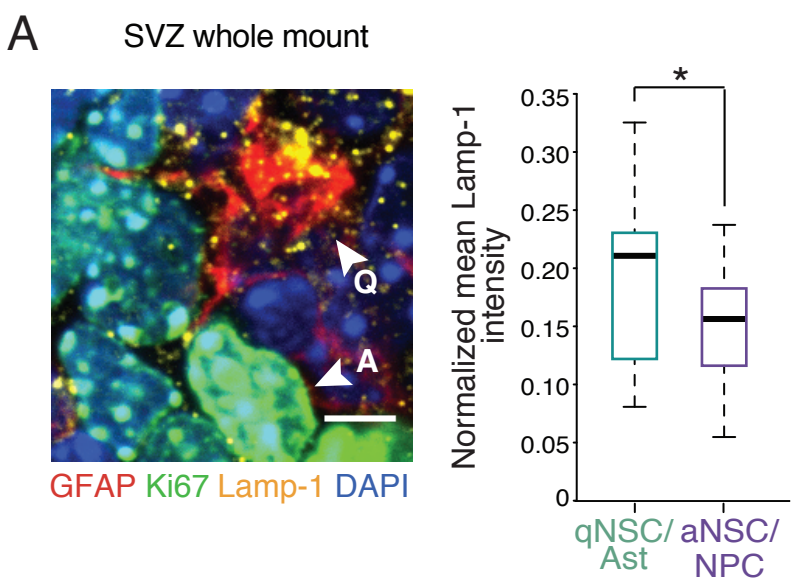
A
SVZ whole mount
Q
A
GFAP Ki67 Lamp-1 DAPI
Normalized mean Lamp-1 intensity
0.35
0.30
0.25
0.20
0.15
0.10
0.05
0
*
qNSC/ Ast
aNSC/ NPC
B
Lysosomal membrane quantification
Normalized Lamp2–positive area per cell
2.0
1.5
1.0
0.5
0.0
**
qNSC
aNSC
C
Relative autolysosome levels
Normalized median mCherry/GFP
2.5
2.0
1.5
1.0
0.5
0.0
***
qNSC
aNSC

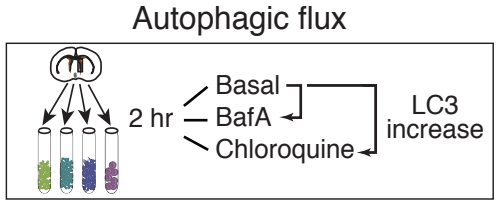
D
Autophagic flux
2 hr
Basal
BafA
Chloroquine
LC3 increase

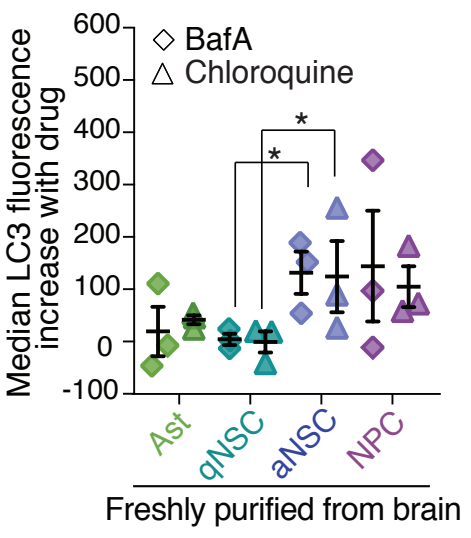
Median LC3 fluorescence increase with drug
600
500
400
300
200
100
0
-100
◇ BafA
△ Chloroquine
*
*
Ast
qNSC
aNSC
NPC
Freshly purified from brain

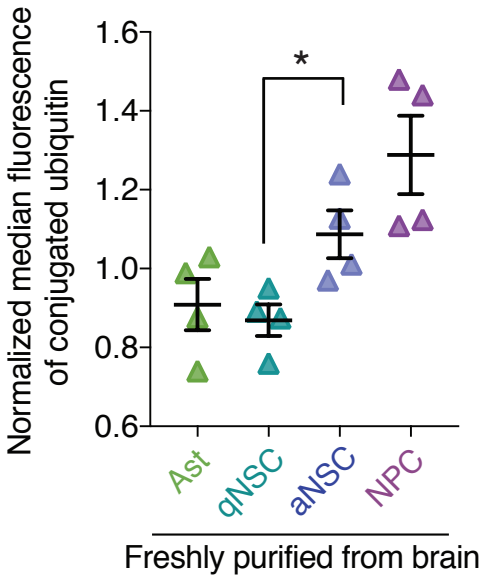
E
Conjugated ubiquitin
Normalized median fluorescence of conjugated ubiquitin
1.6
1.4
1.2
1.0
0.8
0.6
*
Ast
qNSC
aNSC
NPC
Freshly purified from brain

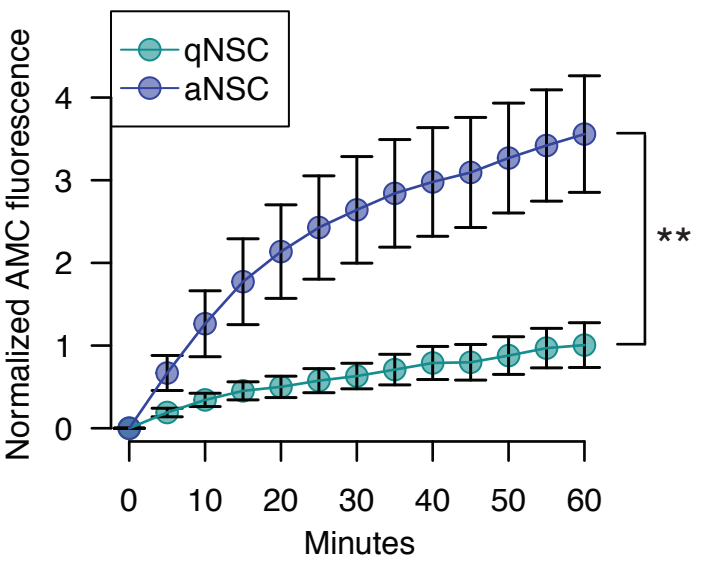
F
Chymotrypsin-like proteasome activity
Normalized AMC fluorescence
4
3
2
1
0
qNSC
aNSC
**
0
10
20
30
40
50
60
Minutes

Figure S6

A

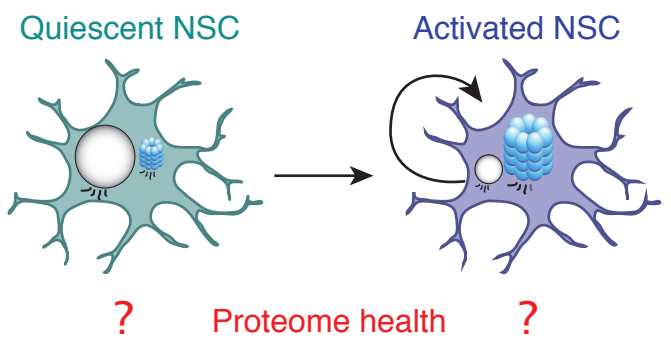

B

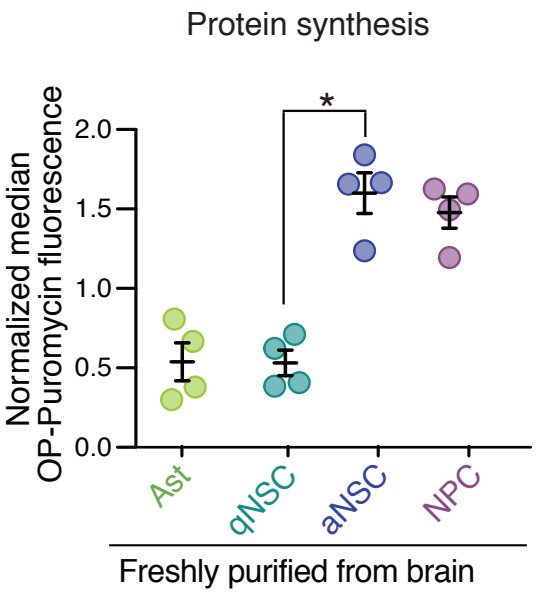

C Aggregate isolation by differential solubility

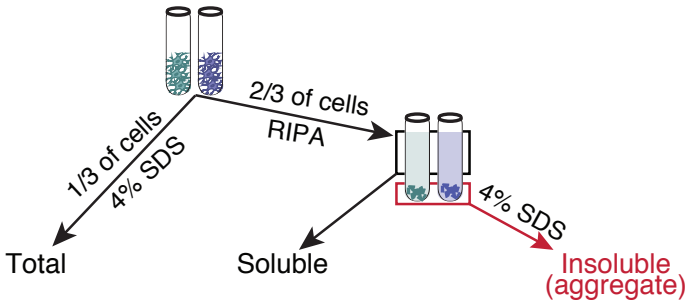

D Total insoluble fraction

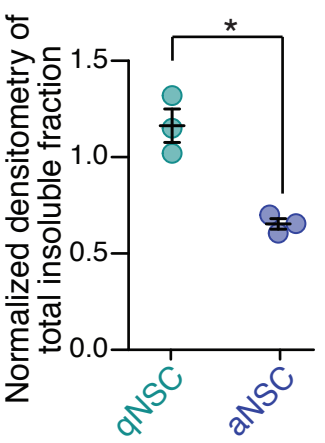

E High molecular weight insoluble fraction

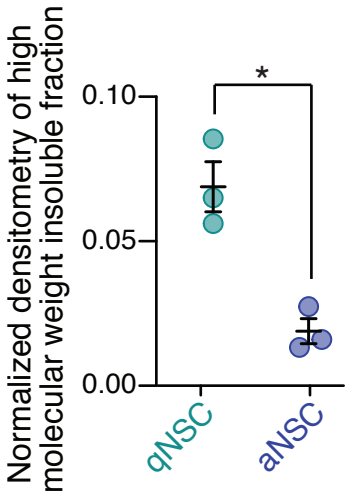

Figure S7

A

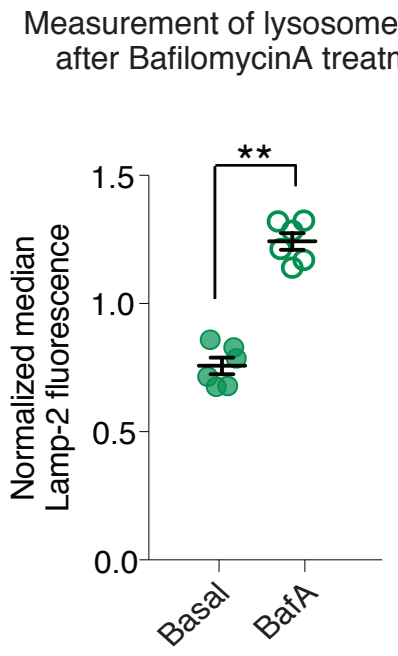

B

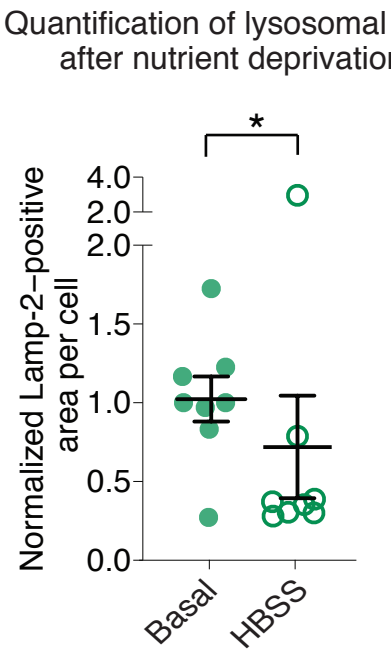

C

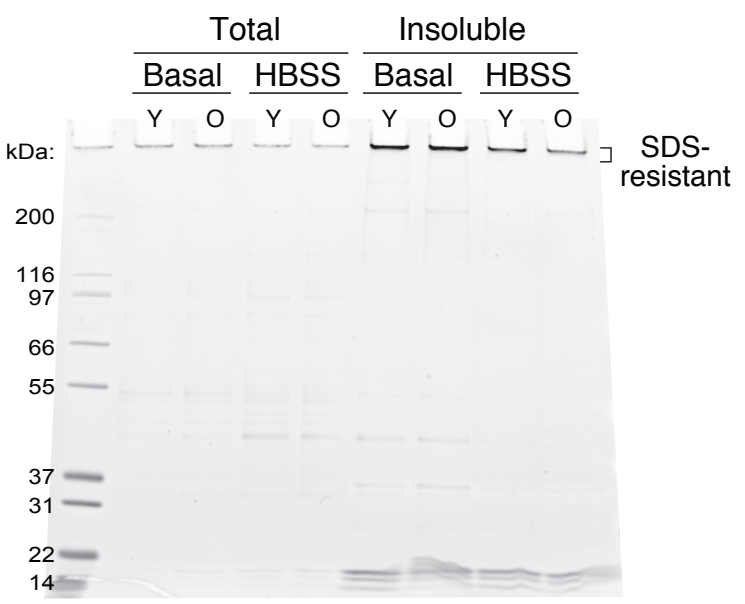

D

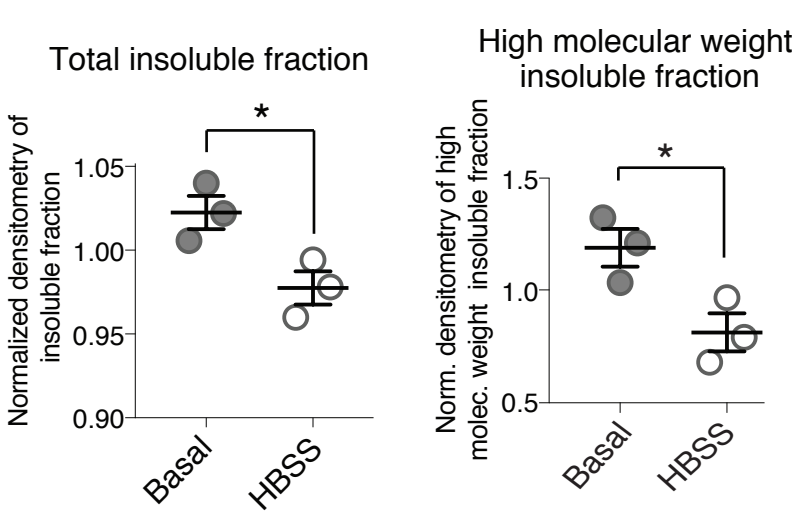

E

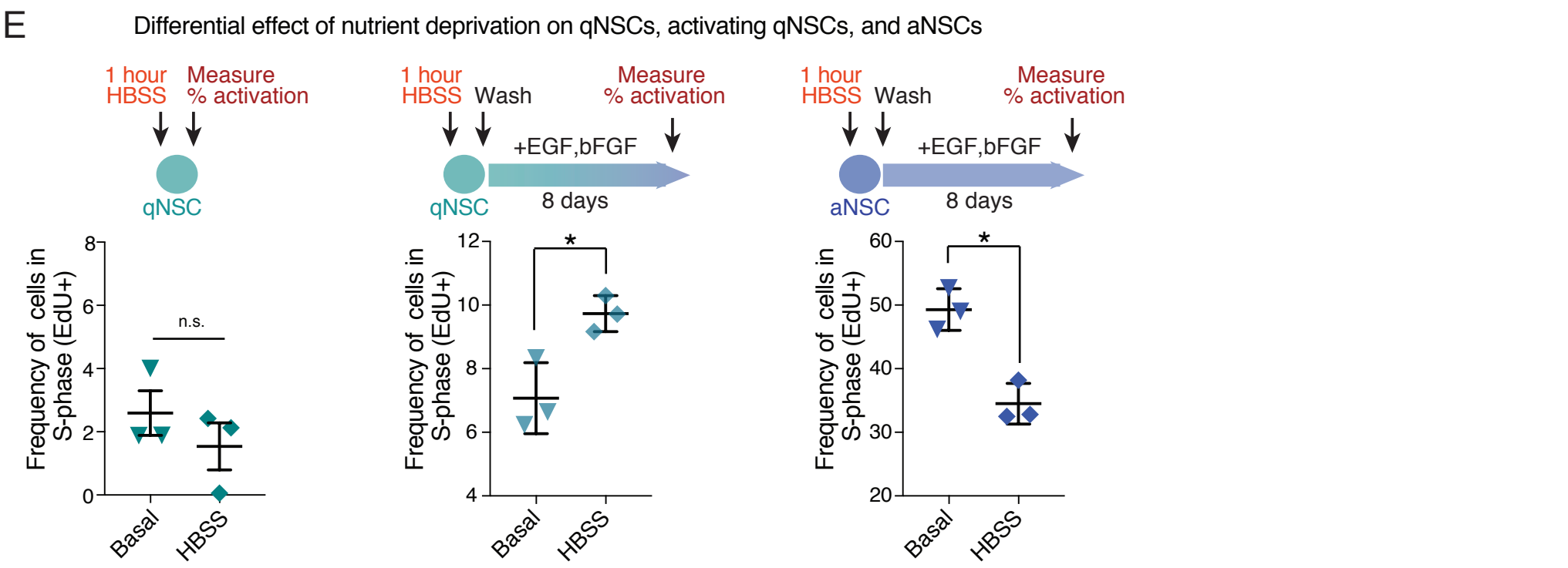

F

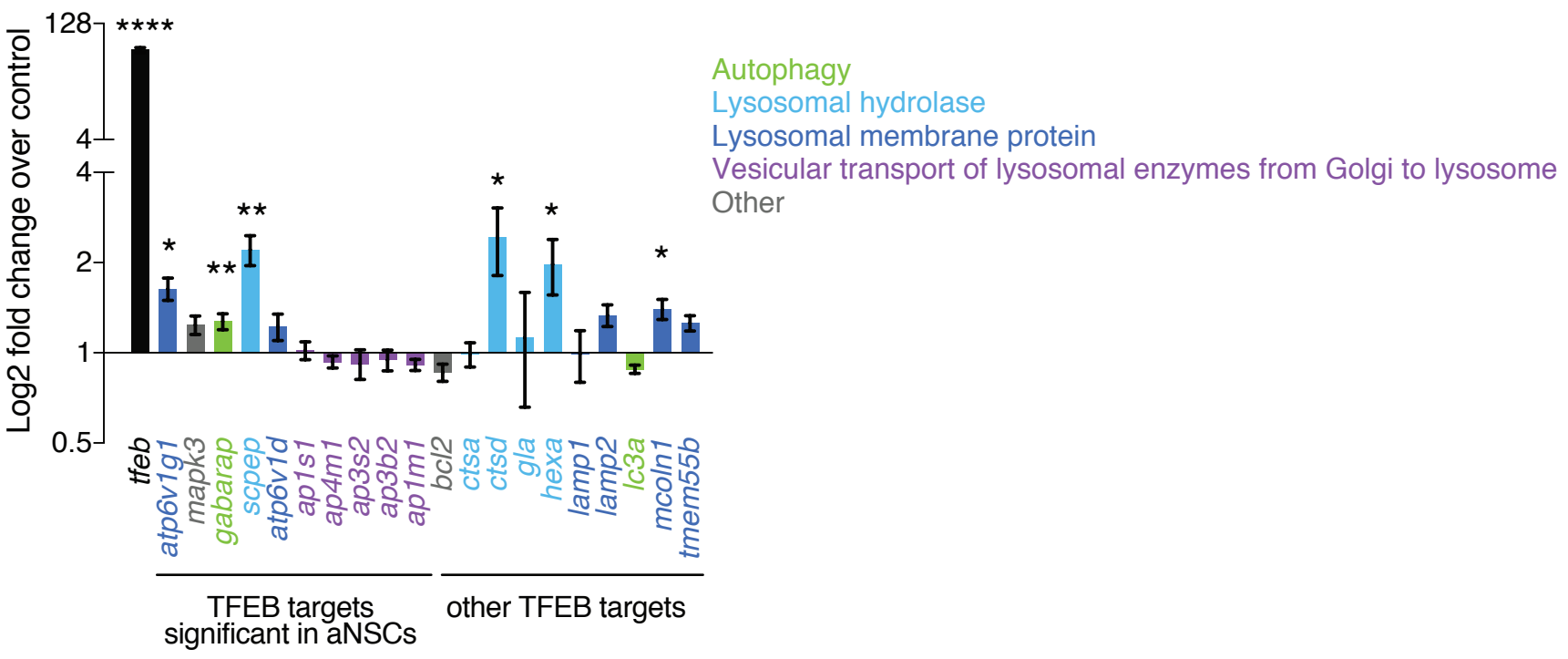

Figure S8

A

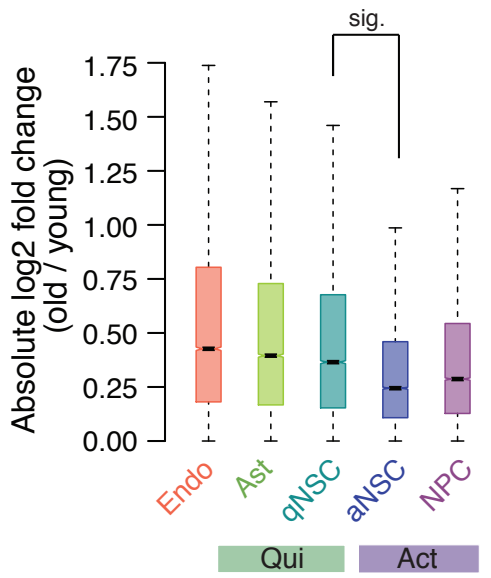

C

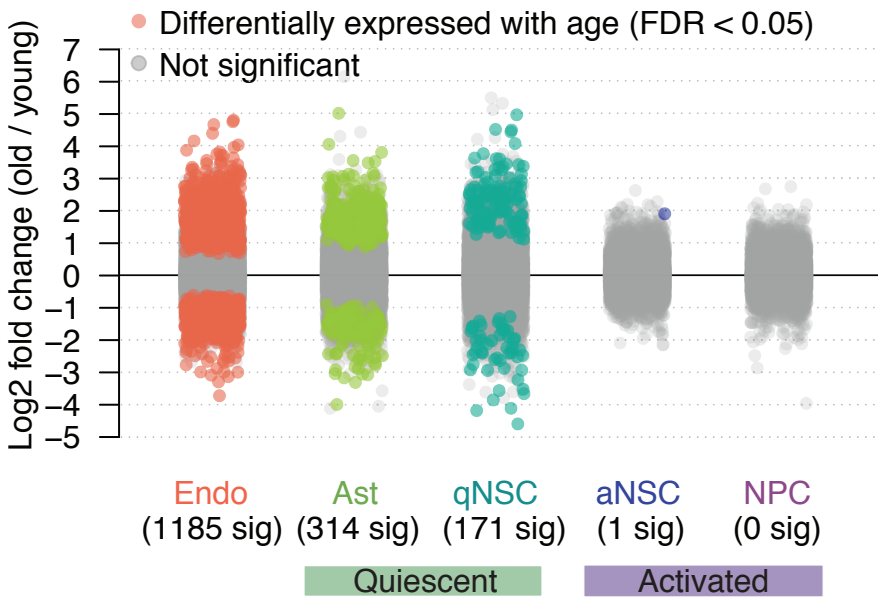

B

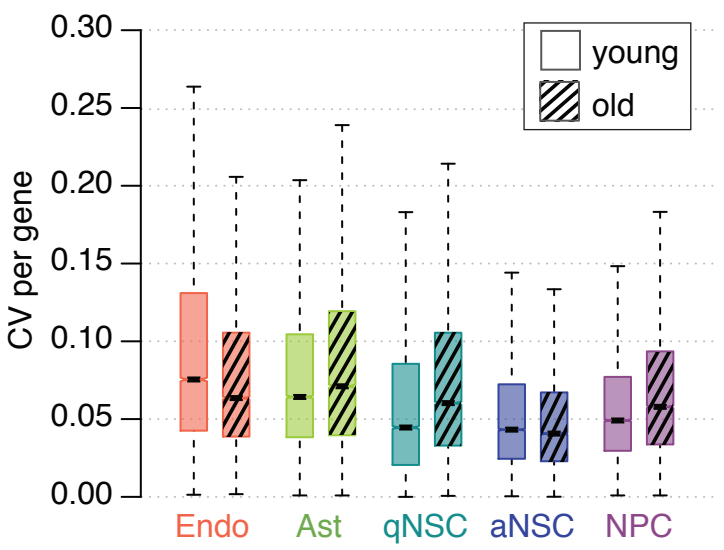

D

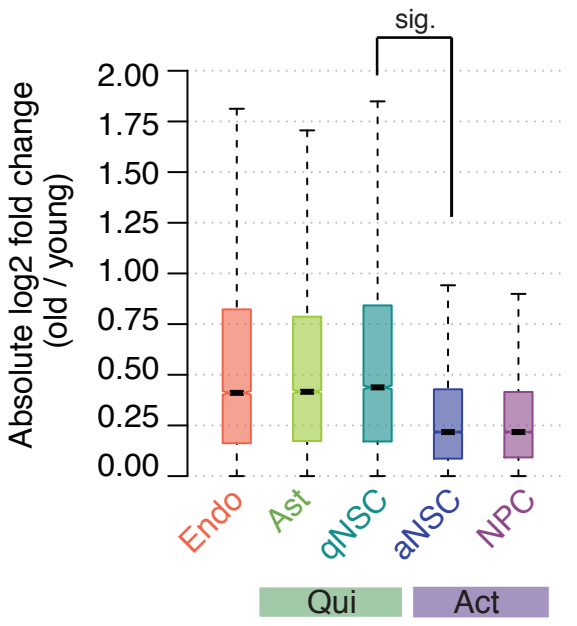

E

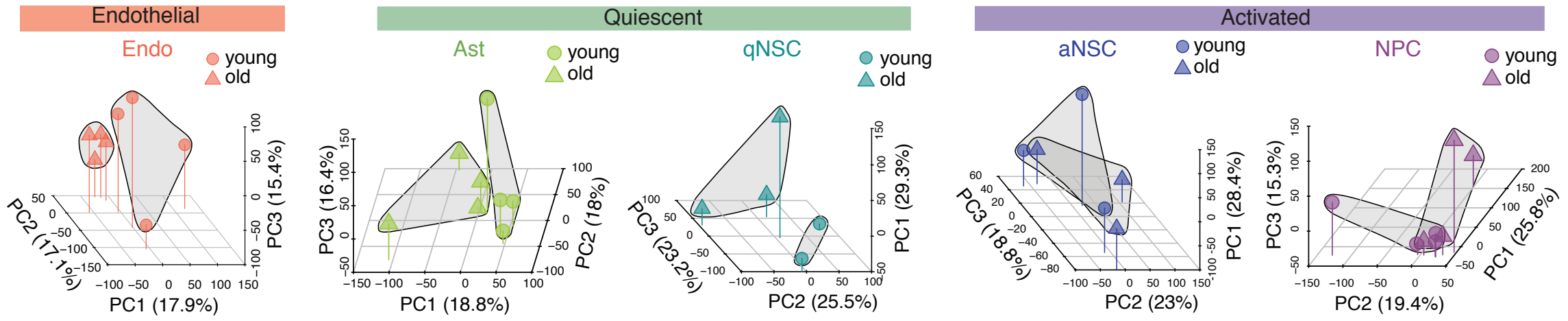

F

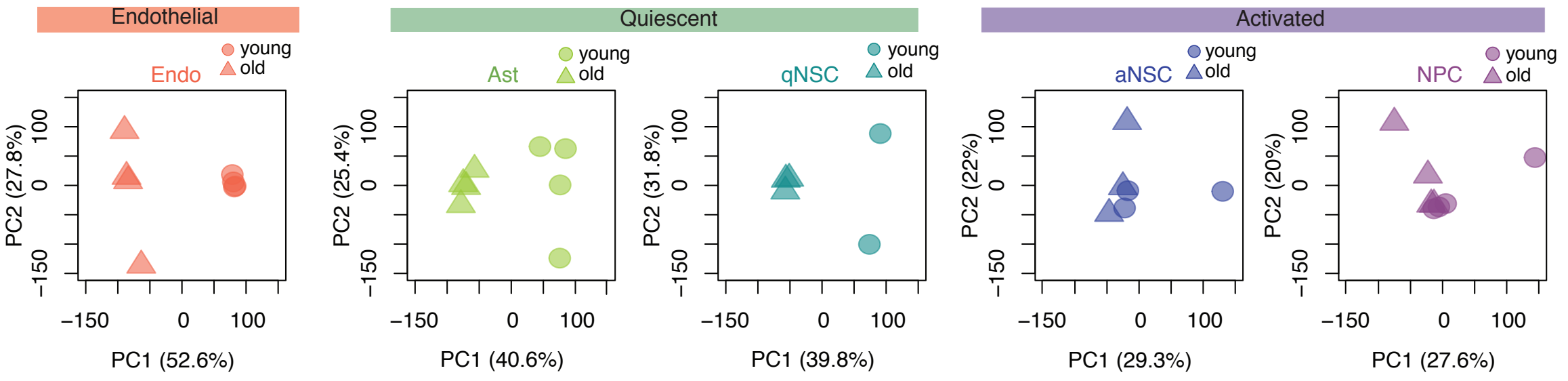

G

In vivo differential gene expression with age of protein homeostasis pathways

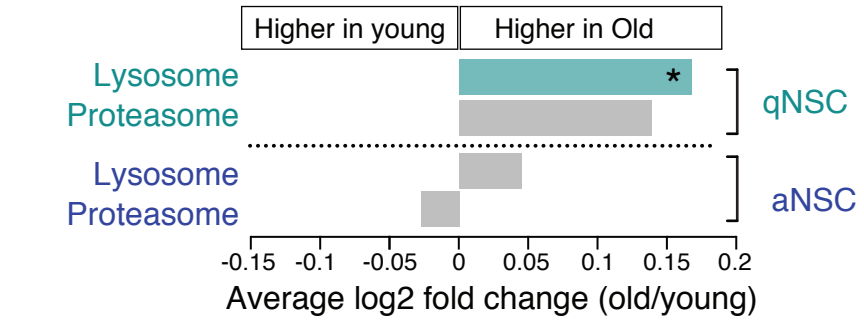

Figure S9

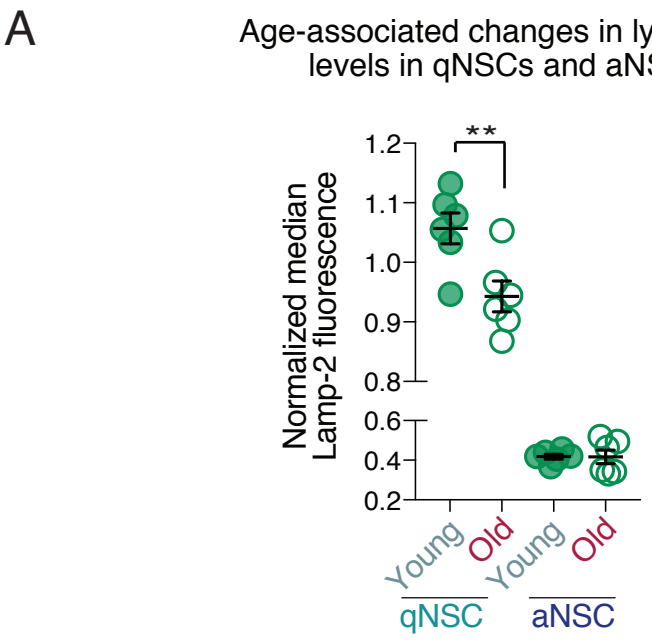
A
Age-associated changes in lysosome levels in qNSCs and aNSCs
Normalized median Lamp-2 fluorescence
1.2
1.1
1.0
0.9
0.8
0.6
0.4
0.2
**
Young
Old
Young
Old
qNSC
aNSC

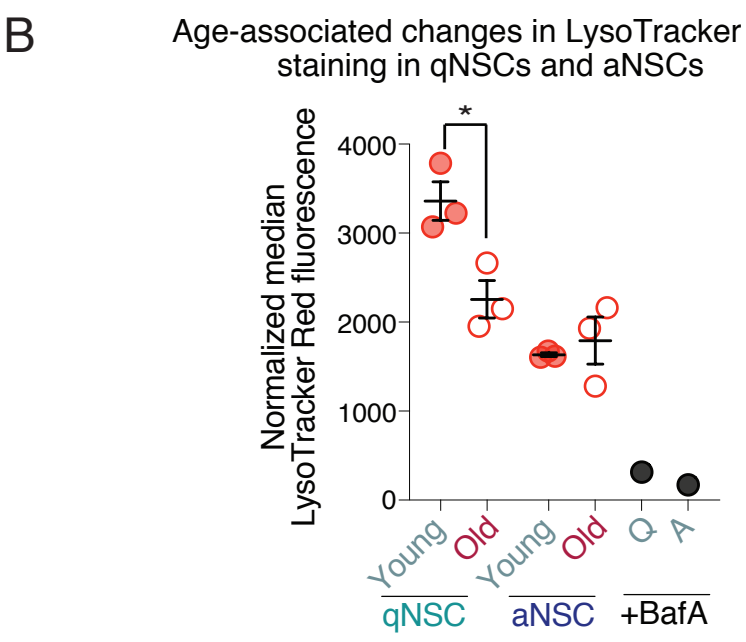
B
Age-associated changes in LysoTracker Red staining in qNSCs and aNSCs
Normalized median LysoTracker Red fluorescence
4000
3000
2000
1000
0
*
Young
Old
Young
Old
Q
A
qNSC
aNSC
+BafA

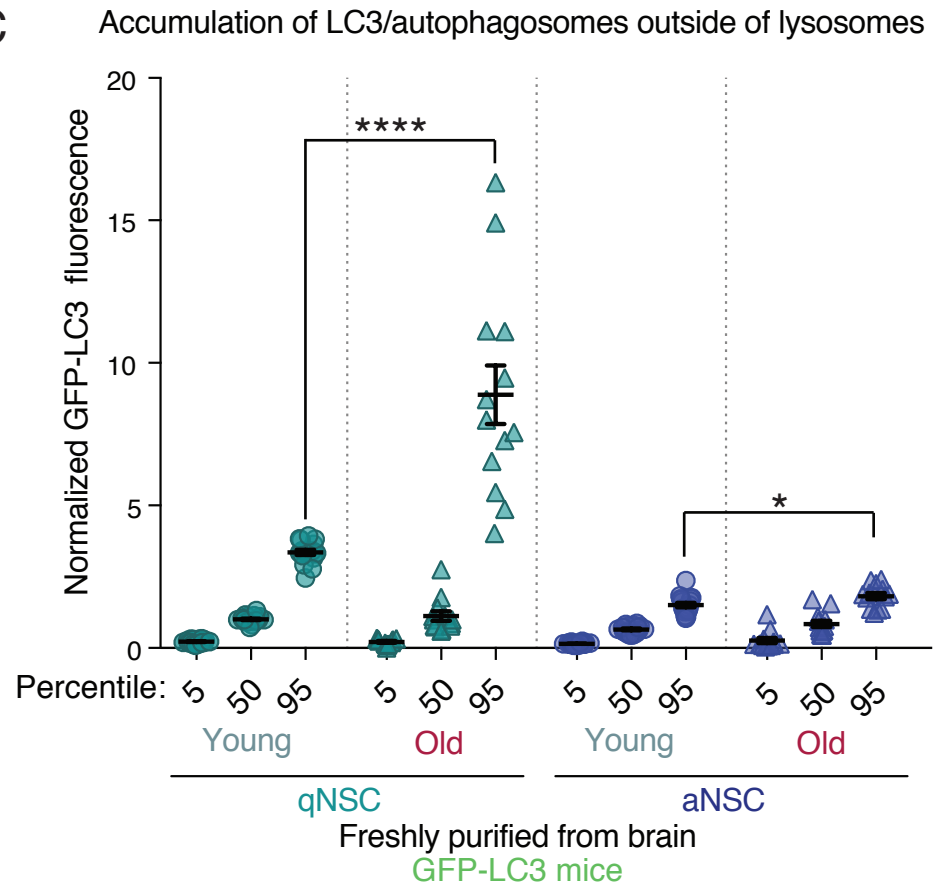
C
Accumulation of LC3/autophagosomes outside of lysosomes
Normalized GFP-LC3 fluorescence
20
15
10
5
0
****
*
Percentile: 5 50 95 5 50 95 5 50 95 5 50 95
Young
Old
Young
Old
qNSC
aNSC
Freshly purified from brain
GFP-LC3 mice

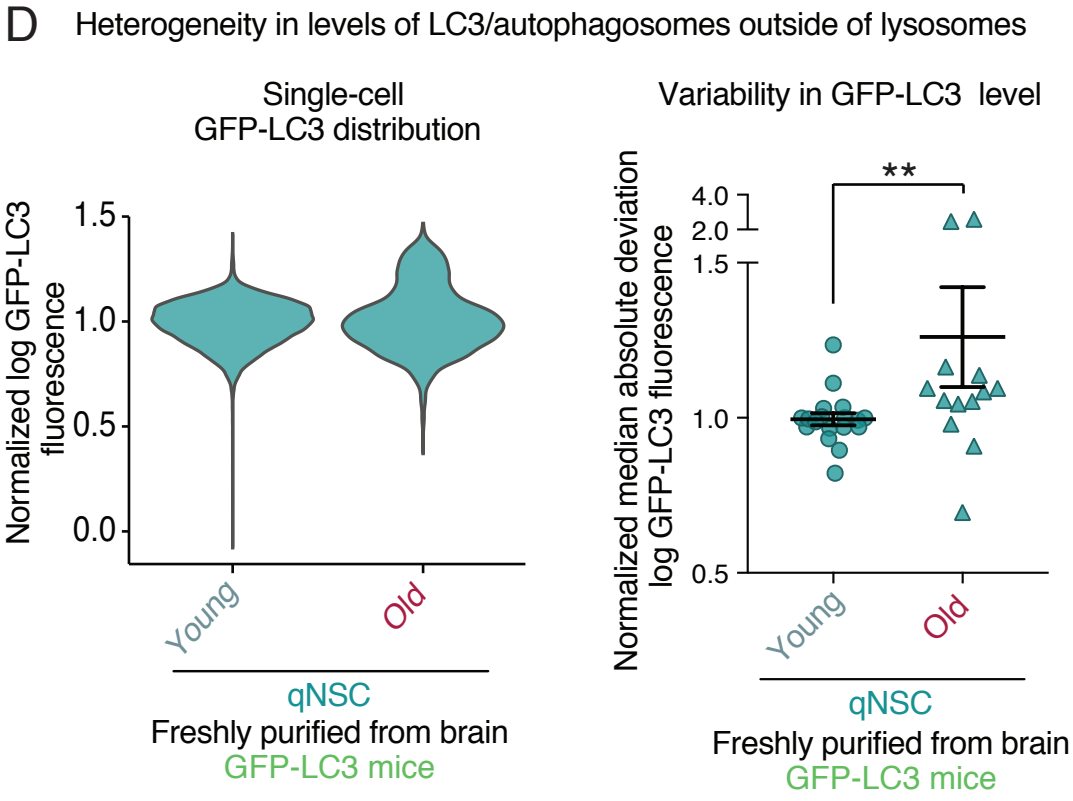
D
Heterogeneity in levels of LC3/autophagosomes outside of lysosomes
Single-cell GFP-LC3 distribution
Normalized log GFP-LC3 fluorescence
1.5
1.0
0.5
0.0
Young
Old
qNSC
Freshly purified from brain
GFP-LC3 mice
Variability in GFP-LC3 level
Normalized median absolute deviation log GFP-LC3 fluorescence
4.0
2.0
1.5
1.0
0.5
**
Young
Old
qNSC
Freshly purified from brain
GFP-LC3 mice

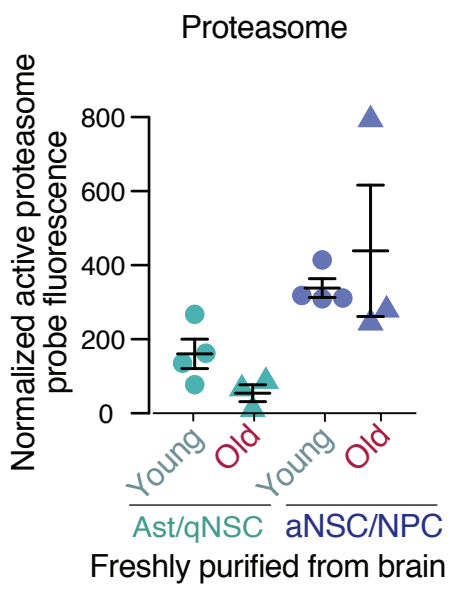
E
Proteasome
Normalized active proteasome probe fluorescence
800
600
400
200
0
Young
Old
Young
Old
Ast/qNSC
aNSC/NPC
Freshly purified from brain

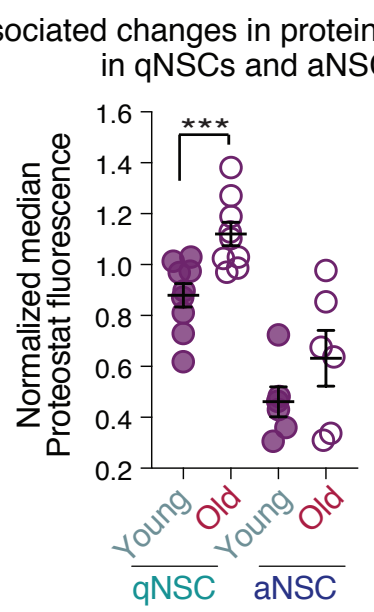
F
Age-associated changes in protein aggregate levels in qNSCs and aNSCs
Normalized median Proteostat fluorescence
1.6
1.4
1.2
1.0
0.8
0.6
0.4
0.2
***
Young
Old
Young
Old
qNSC
aNSC

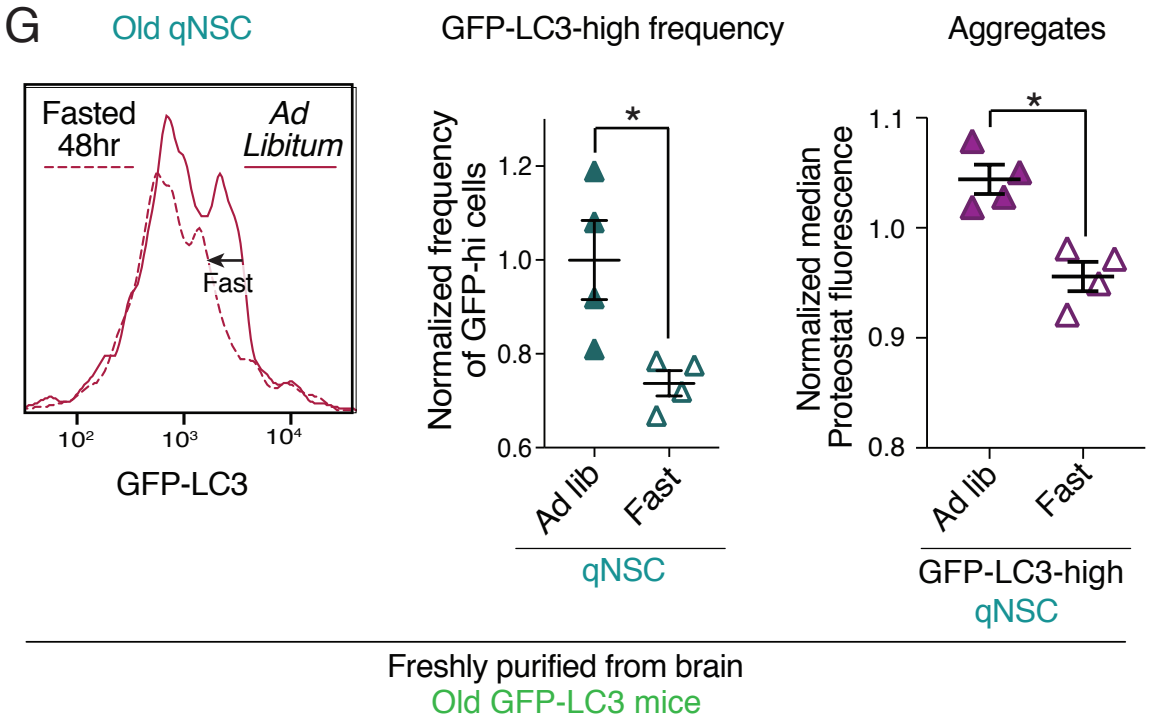
G
Old qNSC
Fasted 48hr
Ad Libitum
Fast
10²
10³
10⁴
GFP-LC3
GFP-LC3-high frequency
Normalized frequency of GFP-hi cells
1.2
1.0
0.8
0.6
*
Ad lib
Fast
qNSC
Aggregates
Normalized median Proteostat fluorescence
1.1
1.0
0.9
0.8
*
Ad lib
Fast
GFP-LC3-high qNSC
Freshly purified from brain
Old GFP-LC3 mice

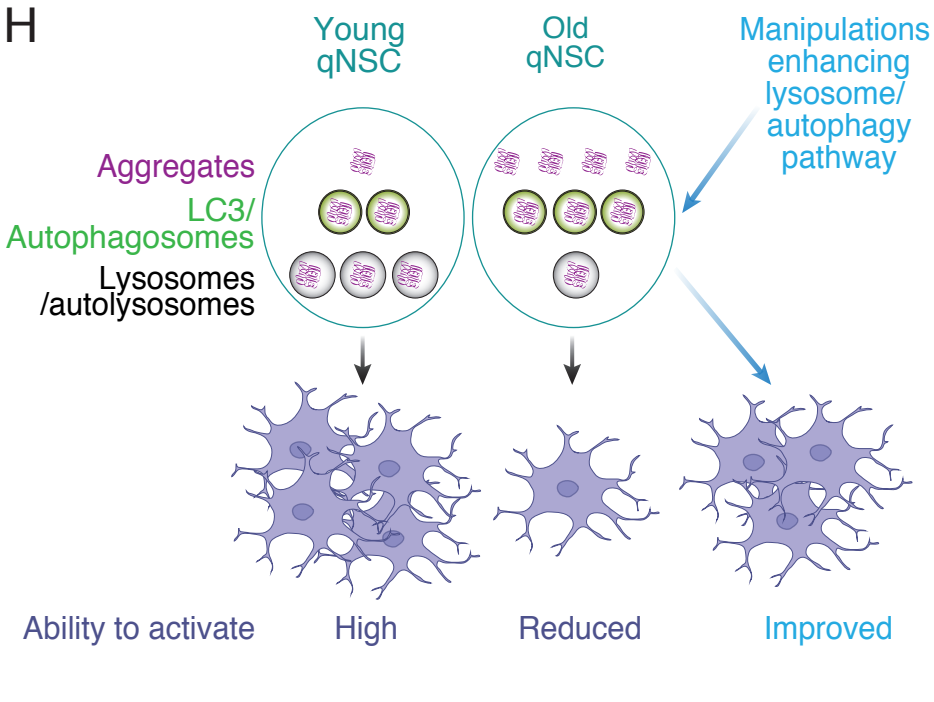
H
Young qNSC
Old qNSC
Manipulations enhancing lysosome/ autophagy pathway
Aggregates
LC3/ Autophagosomes
Lysosomes /autolysosomes
Ability to activate
High
Reduced
Improved